Journal Pre-proof

Design, synthesis and evaluation of novel thienopyrimidine-based agents bearing diaryl urea functionality as potential inhibitors of angiogenesis

Aram Faraji, Tayebeh Oghabi Bakhshaiesh, Zaman Hasanvand, Rasoul Motahari, Elahe Nazeri, Mohammad Amin Boshagh, Loghman Firoozpour, Hossein Mehrabi, Ali Khalaj, Rezvan Esmaeili, Alireza Foroumadi

PII: S0223-5234(20)30914-4

DOI: https://doi.org/10.1016/j.ejmech.2020.112942

Reference: EJMECH 112942

To appear in: *European Journal of Medicinal Chemistry*

Received Date: 29 June 2020

Revised Date: 10 October 2020

Accepted Date: 11 October 2020

Please cite this article as: A. Faraji, T.O. Bakhshaiesh, Z. Hasanvand, R. Motahari, E. Nazeri, M.A. Boshagh, L. Firoozpour, H. Mehrabi, A. Khalaj, R. Esmaeili, A. Foroumadi, Design, synthesis and evaluation of novel thienopyrimidine-based agents bearing diaryl urea functionality as potential inhibitors of angiogenesis, *European Journal of Medicinal Chemistry*, https://doi.org/10.1016/j.ejmech.2020.112942.

Design, synthesis and evaluation of novel thienopyrimidine-based agents bearing diaryl urea functionality as potential inhibitors of angiogenesis

Aram Faraji [a], Tayebeh Oghabi Bakhshaiesh [b], Zaman Hasanvand [a], Rasoul Motahari [a], Elahe Nazeri [b], Mohammad Amin Boshagh [b], Loghman Firoozpour [c], Hossein Mehrabi [d], Ali Khalaj [a], Rezvan Esmaeili [b,*], Alireza Foroumadi [a, c, **]

[a] *Department of Medicinal Chemistry, Faculty of Pharmacy, Tehran University of Medical Sciences, Tehran, Iran*

[b] *Genetics Department, Breast Cancer Research Center, Motamed Cancer Institute, ACECR, Tehran, Iran*

[c] *Drug Design and Development Research Center, The Institute of Pharmaceutical Sciences (TIPS), Tehran University of Medical Sciences, Tehran, Iran*

[d] *Department of Chemistry, Vali-e-Asr University of Rafsanjan, 77176 Rafsanjan, Iran*

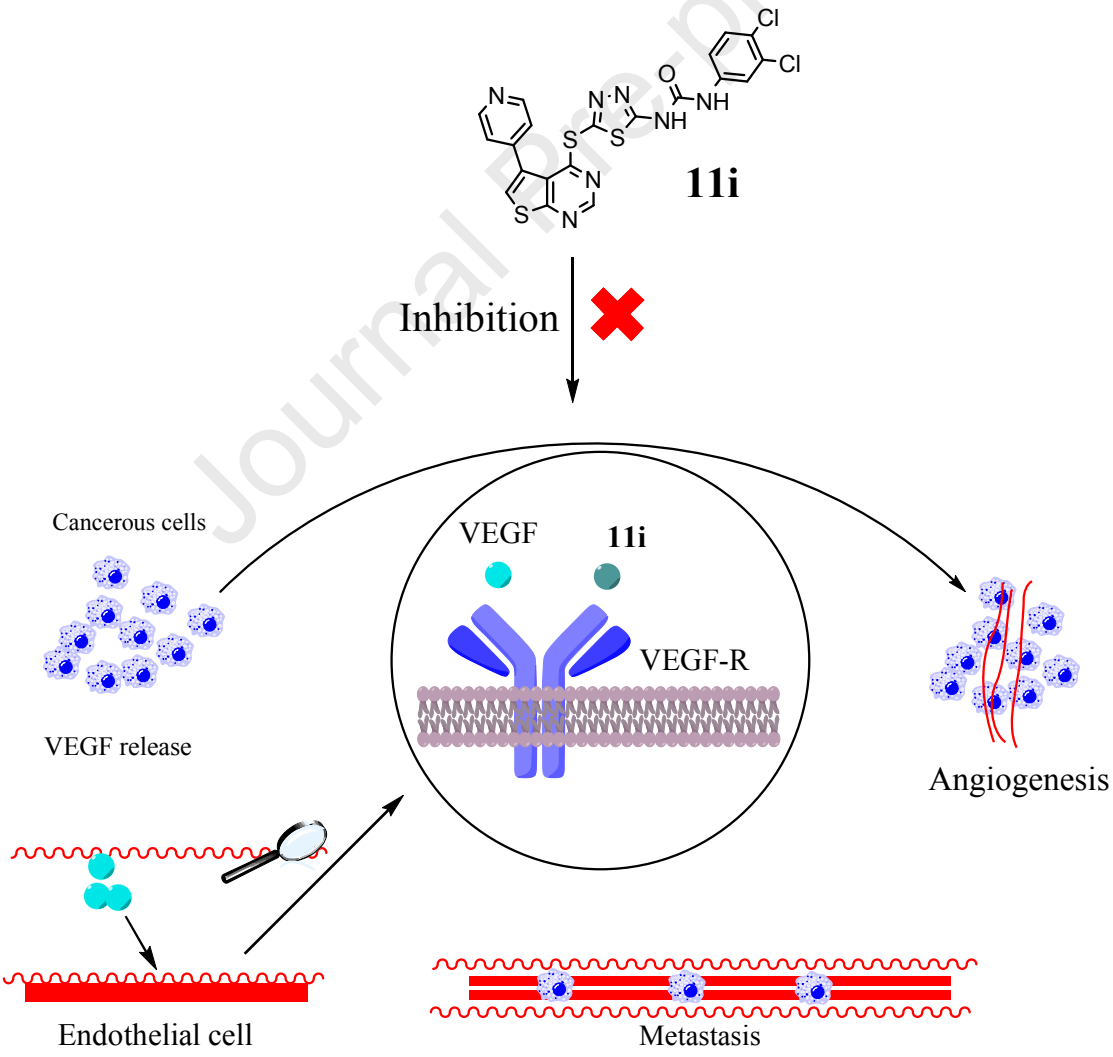

Design, synthesis and evaluation of novel thienopyrimidine-based agents bearing diaryl urea functionality as potential inhibitors of angiogenesis

Aram Faraji [a], Tayebeh Oghabi Bakhshaiesh [b], Zaman Hasanvand [a], Rasoul Motahari [a], Elahe Nazeri [b], Mohammad Amin Boshagh [b], Loghman Firoozpour [c], Hossein Mehrabi [d], Ali Khalaj [a], Rezvan Esmaeili [b,*], Alireza Foroumadi [a, c, **]

[a] *Department of Medicinal Chemistry, Faculty of Pharmacy, Tehran University of Medical Sciences, Tehran, Iran*

[b] *Genetics Department, Breast Cancer Research Center, Motamed Cancer Institute, ACECR, Tehran, Iran*

[c] *Drug Design and Development Research Center, The Institute of Pharmaceutical Sciences (TIPS), Tehran University of Medical Sciences, Tehran, Iran*

[d] *Department of Chemistry, Vali-e-Asr University of Rafsanjan, 77176 Rafsanjan, Iran*

Abstract:

Inhibition of angiogenesis is a promising strategy for the treatment of cancer. Herein, we describe the design and synthesis of thieno[2,3-*d*]pyrimidine-1,3,4-thiadiazole-aryl urea derivatives **11a-m** to evaluate their efficacy in the chick chorioallantoic membrane (CAM) assay. Among target agents, **11i** had a considerable activity against prostate cancer cell line, PC3 (IC_{50} = 3.6 μM). Moreover, induction of apoptosis, good inhibitory activity against the growth of capillary blood vessels, and inhibition of VEGFR-2 phosphorylation were noticeable parameters which convinced us that **11i** could be considered as a promising candidate for the discovery of novel drugs to treat tumors, particularly prostate cancer.

Keywords: Angiogenesis, Thieno[2,3-*d*]pyrimidine, 1,3,4-Thiadiazole, CAM assay, PC3, Apoptosis, VEGFR-2

* Corresponding author.
Tel: 98 21 88796003; Fax: 98 21 88796003. E-mail: esmaeili.rezvan@gmail.com (R. Esmaeili)

** Corresponding author.
Tel.: 98 21 66406757; Fax: 98 21 66461178. E-mail: aforoumadi@yahoo.com (A. Foroumadi)

1. Introduction

Cancer is the second lethal disease all around the world. According to World Health Organization (WHO) reports, 9.6 million cancer deaths occurred in 2018. Regarding the increasing rate of cancer prevalence, a great deal of effort in medicinal chemistry has been taken toward design and synthesis of potential anti-cancer agents [1]. A considerable part of ongoing research has been focused on providing novel targets controlling certain signaling pathways attributed to cancer cell proliferation and propagation. Angiogenesis, process of new blood vessel formation, is vital for cell development and reproduction. Considering the similar function in cancerous cells, angiogenesis plays a significant role in tumor progression and metastasis. Therefore, efficient anti-angiogenesis agents could be considered as promising strategy for cancer treatment [2].

Growth factors, including vascular endothelial growth factors (VEGFs) and their receptors (VEGFRs) regulate angiogenesis. Among three subtypes of VEGFRs, VEGFR-2 plays the most substantial role in the tumor angiogenesis. VEGF-VEGFR-2 interaction leads dimerization and subsequently autophosphorylation of tyrosine (Tyr1054 and Tyr1059) in receptor resulted into angiogenesis signaling pathways in tumor environment [3]. Therefore, antitumor agents interfering with tyrosine phosphorylation have inhibitory activity in angiogenesis. In addition to VEGFR-2, tyrosine-protein kinase receptor (Tie-2) and erythropoietin producing hepatocyte receptor B4 (EphB4) taking participation in maturation of blood vessels have recently received interest in medicinal chemistry [4].

Over decades, different scaffolds showing VEGFR-2 inhibitory activity have been reported. Among them, compounds having quinazolines, thienopyrimidines, indolines, urea derivatives, as well as pyridine and pyrimidine derivatives have been more prevalent [5-13]. Thieno[2,3-*d*]pyrimidines, in particular, have been found in many natural products and drugs, including Relugolix, PRX-08066, and DDP-225. Moreover, they have shown wide spectrum of biological activities, for example anticancer, kinase inhibition (like VEGFR-2 inhibition, FGFR1 inhibition, B-Raf inhibition, FLT3 inhibition, and EGFR kinase inhibition), antioxidant, anti-inflammatory, antimicrobial, antiviral, antituberculosis, and CNS protection activities [14, 15].

Some drugs containing diaryl urea, including sorafenib, regorafenib, and tivozanib have been approved and marketed as VEGFR-2 inhibitors (Fig. 1). Diaryl ureas have played important role

in VEGFR-2 inhibitory potency; however, they have been modified to evaluate their activities. For example, urea functional group has been replaced by thiourea moiety, as well as oxadiazole, 1,3,4thiadiazole, and 1,2,3-triazole rings to achieve more binding affinity with receptor [16-18]. Additionally, quinazolinones, indazolines, and thieno[2,3-*d*]pyrimidines have been utilized as aryl ring substituent [19-21].

SKLB1002, quinazoline bearing 1,3,4-thiadiazole, has been identified as potent VEGFR-2 inhibitor with minimum toxicity [22-23]. In present study, SKLB1002 and sorafinib have been employed to design a novel series of thieno[2,3-*d*]pyrimidine-1,3,4-thiadiazole-aryl urea derivatives **11a-m** (Fig. 2). Two major modifications have been introduced based on known VEGFR-2 inhibitors: quinazoline ring of SKLB1002 has been replaced with its bioisoster, thieno[2,3-*d*]pyrimidine. Moreover, aromatic ring linker in Sorafinib has been replaced with 1,3,4-thiadiazole moiety.

2. Chemistry

The synthetic approach toward target products **11a-m** has been outlined in Scheme 1. Gewald reaction using 4-acetylpyridine **1**, ethyl cyanoacetate **2**, and sulfur **3** was applied to prepare multi-substituted thiophene **4** [24,25] which subsequently underwent cyclization by formamidine acetate to form thieno[2,3-*d*]pyrimidin skeleton **5**. The chlorination of carbonyl group in this moiety with phosphoryl chloride was carried out to obtain compound **6**. On the other hand, the reaction between thiosemicarbazide **7** and carbon disulfide **8** afforded 5-amino-1,3,4-thiadiazole-2-thiol **9** followed by condensation with substituted phenyl isocyanates to obtain compounds **10**. Finally, nucleophilic aromatic substitution between chlorine moiety compound **6** and corresponding diaryl urea **10** was performed to synthesize desirable products **11a-m**.

3. Results and Discussion

3.1. The cytotoxic activity

Synthesized thieno[2,3-*d*]pyrimidine-1,3,4-thiadiazole-aryl urea derivatives **11a-m** were evaluated for their anti-proliferative activities against PC3, HepG2, T47D, and HUVEC. The results were summarized in Table 1. The IC_{50} values against the PC3 cell line revealed that the target compounds showed significant cytotoxic activity at concentrations less than 13 μM. In other words, all final products, without exception, were more potent than the positive control. Compound **11h**, bearing a fluorine substituent at the para position had the best anti-proliferative

activity against PC3. Furthermore, the other three derivatives (**11e**, **11g**, and **11i**) were effective against PC3 and their cytotoxicity should not be ignored. Given that compounds **11e** and **11g** could favorably inhibit the proliferation of PC3 cells, the placement of methyl substituent at the para position contributes presumably to the optimal cytotoxicity against this cancer cell line.

To evaluate the anti-proliferative activity against liver cancer, the HepG2 cell line was selected. What Table 1 does imply is that **11d**, **11e** and **11f** were the best compounds against HepG2. In comparison to the positive control, the final derivatives had a moderate cytotoxic effect against HepG2. Besides, disubstituted derivatives bearing the chlorine atom at the para position (**11i** and **11k**) were the weakest ones against HepG2.

The comparison of IC_{50} values against T47D cells revealed that most of the compounds had minimal potency. Neither para nor meta-methoxy substituted derivatives (**11f** and **11l**) had good anti-proliferative activity against T47D and as Table 1 implies, the IC_{50} values of these derivatives were more than 50 μM. HUVEC (human umbilical vein endothelial cell) cells are exposed to VEGF and involved in the process of angiogenesis. Thus, through the evaluation of cytotoxic effects of the corresponding compounds against HUVEC, their anti-angiogenic activity would be predictable to some extent. The presence of four derivatives (**11b**, **11i**, **11j**, and **11m**) owning IC_{50} values less than 15 μM is an indication of how structures bearing the diaryl urea functionality can affectionately inhibit the proliferation of HUVEC cells and presumably angiogenesis. Compound **11i** was the most potent one with IC_{50} = 7.8 μM.

Preclinical data have revealed that VEGF has a stimulating effect on the proliferation of prostate cancer cells and angiogenesis [26]. In other words, VEGF as an angiogenic factor is involved in the process of neovascularization observed in prostate cancer [27]. Moreover, in present study, results revealed that PC3 cells were more sensitive to compounds **11a-m** in comparison to other three cell lines (HepG2, T47D, and HUVEC). Comparing to sorafinib, compound **11i** was efficiently inhibit PC3, T47D, and HUVEC cell proliferation; however, it did not show good cytotoxic activity against HepG2 cells (IC_{50} = 61.9 μM). Additionally, the cytotoxic effect of compound **11i** against normal fibroblast Hu02 cell line (IC_{50} = 34.3 ± 0.3 μM) was comparable to that of sorafenib (IC_{50} = 40.0 ± 0.5 μM) (Table 2).

3.2. Apoptosis-inducing activity

Apoptosis, the programmed cell death, causes the damaged cells to eliminate. Any perturbation in this physiological process leads to various diseases including cancer. In a general sense, the cell death pathway conducted by anticancer agents is divided into two more pathways: apoptosis and necrosis. In an attempt to figure out which pathway, apoptosis or necrosis, is responsible for killing the cells, a double staining flow cytometry assay using Annexin V-FITC/propidium iodide was carried out. Dimethyl sulfoxide was used as solvent and sorafenib as positive control. Derivatives selected for this purpose included **11h** and **11i** and they were evaluated at their IC_{50} on the PC3 cell line. PC3 cells were affected moderately by compound **11h** so that the population of apoptotic cells was 24.47%. It should be mentioned that one-third of cells (32.2%) were affected by the necrosis. On the other hand, the treatment of PC3 cells with compound **11i** gave rise to severe apoptosis so that nearly 44% of cells were influenced by the programmed cell death. Dimethyl sulfoxide and sorafenib resulted in 10.88% and 18.52% cell apoptosis. As shown in Fig. 3, compound **11i** provoked cell death in an apoptotic pathway.

Given the role of endothelial cells in vascular homeostasis and cancer pathogenesis, the HUVEC cell line was selected to assess the apoptosis-inducing activity of **11i**. As illustrated in Fig. 4, the apoptotic elimination of HUVEC cells was occurred moderately by **11i** (28.45%) which was more than apoptotic cells provoked by sorafenib (19.09%). The percentage of HUVEC cells apprehended in the necrosis phase treated with **11i** was comparatively lower than that of sorafinib (21.0% in comparison with 16.4%).

3.3. Cell cycle analysis

In accordance with the IC_{50} values obtained from Table 1, compounds **11h** and **11i** were selected to be further examined in respect of their effect on the cell cycle progression (Figs.5 and 6). Interference with the normal cell cycle distribution of the PC3 cell line caused by **11h** was noted. A glimpse of the chart as demonstrated in Fig. 6, reveals that compound **11h** could increase the percentage of cells in the G1-phase by 1.26-fold, respectively compared to the control (55.92% *vs* 44.11%). Of course, in comparison with the control (44.12%), the percentage of cells in the S-phase was lower (29.76%). Simultaneously, an increase in the number of cancerous cells in the G1-phase and a decrease in the S-phase is usually indicative of the cell cycle arrest in the G1-phase. Thus, a quantity of PC3 cells treated with **11h** were imprisoned in the G1-phase and couldn’t enter the next one. The cell cycle distribution of PC3 cells exposed to sorafenib showed

similar results so that, it could tremendously increase the number of G1-cells (66.19%) and decrease S-cells (22.32%) as compared with the control (G1= 44.11%, S= 44.12%). However, no meaningful difference was observed between the control (G1= 44.11%, S= 44.12%, G2= 15.97%) and **11i** (G1= 45.23%, S= 40.58%, G2= 12.85%) categories.

In terms of the cell cycle analysis, we often pose the question, whether the cells imprisoned in the subG1-phase are apoptotic or not?

An elevated subG1 cell count has a low predictive value for apoptosis and there is no direct link between the percentage of cells halted in the subG1-phase and the number of apoptotic cells. Analyzing the inducing-apoptosis activity (Fig. 3) and the cell cycle assay (Figs. 5 and 6) indicated the interesting outcomes. As Fig. 7 implies, compound **11i** induced the more significant apoptosis (44%) as compared with **11h** (24.5%). However, the percentage of PC3 cells arrested in the subG1-phase by **11i** (4.38%) was fewer than **11h** (9.73%). Also, in conformity with findings obtained from Fig. 3, it is understandable that in comparison with **11i** (12.6%), the induction of the necrosis phase by **11h** (32%) was more significant. Thus, there is no direct relation necessarily on every occasion between the cell population arrested in the subG1-phase and the amount of induced apoptosis.

The corresponding analysis was performed to evaluate the extent of DNA damage and the percentage of HUVEC cells in various phases (subG1, G1, S, and G2/M) of the cell cycle. Interestingly, the results of the HUVEC cell cycle analysis were the same one observed in the PC3 cell line. As shown in Fig. 8, sorafenib increased tremendously the number of G1-cells (58.69%) and decreased S-cells (27.1%) as compared with the control (G1= 40.93%, S= 41.49%). However, no meaningful difference was observed between the control (G1= 40.93%, S= 41.49%, G2= 6.25%) and **11i** (G1= 48.3%, S= 49.8%, G2= 5.53%) categories. Although the apoptosis was induced by **11i** in PC3 and HUVEC cell lines, the subG1-peak was not observable in the corresponding diagrams of the cell cycle analysis (Figs. 5c and 8b). On the other hand, as a result of the treatment of PC3 and HUVEC cells with **11i**, the cell cycle distribution was not altered as compared with the control. In this manner, the apoptosis is induced probably in all cell subpopulations (G1, S, and G2/M) equally.

3.4. Anti-vascular effects

With regard to the anti-proliferative activity of target compounds against the HUVEC cell line and the analysis of IC_{50} values, superior derivatives (**11b**, **11h**, **11i**, **11j**, and **11m**) were selected to survey the vascular disrupting effect. The chick chorioallantoic membrane (CAM) assay was utilized to assess two aspects of the capillary blood vessels; the number and the length of vessels. As illustrated in Fig. 9, compound **11i** could tremendously reduce the number of capillary blood vessels (65%), which was comparable to sorafenib as the positive control (64%). The inhibitory activity of **11m** was partially satisfactory (35%), even though a substantial reduction was not observed when CAM was exposed to **11b** (29%), **11h** (27%), and **11j** (21%) (Fig. 10a).

The effects of corresponding compounds on the length of the capillary blood vessels were nearly identical to those illustrated in Fig. 10a. As Fig. 10b does imply, **11i** could reduce the length of the vessels to a degree (46%) not seen with other evaluated derivatives. In this context, the effect of sorafenib was almost similar to **11i**.

3.5. Effect on VEGFR-2 phosphorylation

Disruption in the VEGF signaling pathway is a key prerequisite for the inhibition of angiogenesis. On the other hand, as demonstrated through the CAM assay, it was confirmed that **11i** is capable of inhibiting angiogenesis. Thus, the Western blot analysis was implemented to identify the mechanism of action by which **11i** prevents the growth of the capillary blood vessels. As Fig. 11 does imply, in a time-dependent manner, **11i** could reduce massively the levels of phosphorylated form of VEGFR-2. The nearly same effect was achieved with sorafenib. However, after 48 h, the reduced level of p-VEGFR-2 by **11i** was a little more than sorafenib.

The Western blotting was performed also in a concentration-dependent manner. The PC3 cells were exposed to three different concentrations of **11i** (2.4 μM, 3.6 μM, and 5.4 μM) and incubated for 48 h. Cell lysates were blotted against VEGFR-2 and p-VEGFR-2. As reflected in Fig. 12, the phosphorylation of VEGFR-2 was disturbed in a concentration-dependent manner so that a perceptible reduction of band size has occurred in the term of 5.4 μM concentration.

These outcomes give an explanation to the sensational anti-angiogenic activity of **11i** and show a logical connection between the inhibition of angiogenesis and disruption of the VEGF signaling. Ideally, the normalization control (β-actin) was present at constant levels in every sample.

3.6. Molecular docking study

Docking runs were carried out by AutoDock 4.2 with Lamarckian genetic algorithm (LGA) and each Lamarckian job compromised of 50 runs. The co-crystal structure of VEGFR-2 and sorafenib (3WZE) with 1.90 Å resolution was selected and compound **11i** was docked into the active site of the receptor.

The scientific results reported by Okamoto et al. provide an admirable overview of the binding mode of sorafenib and lenvatinib. Across the sorafenib and lenvatinib molecules, two hydrogen bonding interactions can be observed between the urea carbonyl and Asp1046 and the urea NH and Glu885 [28]. Molecular dynamics (MD) simulation suggests that the hydrogen bond engaging Asp1046 is sufficiently stable and is almost preserved throughout the MD simulation time. However, the bifurcated hydrogen bonds involving Glu885 occur occasionally [29]. As illustrated in Fig. 13, the same interactions are observable between **11i** and the receptor. The MM2 methodology was used to determine the free energy of binding. The calculated free energy of binding for **11i** and sorafinib were -8.49 and -8.57 kcal/mol, respectively. It confirmed compound 11i would form greater interactions with active site of the receptor.

4. Conclusion

In conclusion, a novel series of thienopyrimidine-based agents possessing 1,3,4-thiadiazole-aryl urea derivatives **11a-m** were designed, synthesized, and evaluated as potential inhibitors of cell proliferation and angiogenesis. The MTT assay demonstrated that all synthesized compounds had more potent anti-proliferative activity than sorafenib against the PC3 cell line. Compound **11i** (IC_{50}= 3.6 μM) was efficiently induced apoptosis (44% in PC3 cells and 28.45% in HUVEC cells) comparing to standard drug sorafenib. Moreover, compound **11i** showed the noticeable angiogenesis and VEGFR-2 inhibitory activity. Regarding our results, compound **11i** can be considered as a promising candidate for the treatment of metastatic prostate cancer. However, the tumor xenograft model can be helpful to obtain more accurate information.

5. Experimental section

5.1. General chemistry

All starting materials, reagents and solvents were purchased from Merck and Aldrich companies without any purification. The reaction progress and the purity of synthesized compounds were monitored by thin-layer chromatography (TLC) on silica gel 250-micron F254 plastic sheets. Flash chromatography was performed for more purification of chlorine intermediate (**6**) by using

230-400 mesh silica gel and the indicated solvent system. The melting points were determined by Electrothermal IA9100 apparatus and are uncorrected. IR spectra were obtained on *Perkin-Elmer* Spectrum Version *10.03.06* (potassium bromide disks). Nuclear magnetic resonance (NMR) spectra were performed on Varian 500, Bruker 400, and Bruker 300 (TMS as IS). Chemical shifts were reported in parts per million (ppm), downfield from tetramethylsilane. Proton coupling patterns were described as singlet (s), doublet (d), triplet (t), quartet (q), multiplet (m), and broad (b). The mass spectra were run on a Finigan TSQ-70 spectrometer (Finigan, USA) at 70 eV. The elemental analysis for C, H, and N was carried out with an elemental analyzer GmbH VarioEL.

*5.1.1. Ethyl 2-amino-4-(pyridin-4-yl)thiophene-3-carboxylate (**4**)*

A mixture of 4-acetylpyridine (**1**) (14.5 ml, 130.2 mmol), ethyl cyanoacetate (**2**) (15.3 ml, 143.2 mmol) and morpholine (2.25 ml, 26 mmol) was stirred in EtOH at 60-70 ^{o}C for 30 min. Then, sulfur (**3**) (5 g, 156.25 mmol) was added portion by portion over 5 min. The resulting mixture was refluxed under an argon atmosphere overnight. After the consumption of starting materials, cool water was added and the precipitated solid was filtered, washed with n-hexane and allowed to dry to acquire compound **4**, 22.6 g in 70% yield. Yellow solid; mp: 200 ^{o}C; IR (KBr, cm^{-1}): 3396, 3039, 1660, 1607, 1499,1474, 1363; ^{1}H NMR (500 MHz, DMSO-d_6) δ: 8.49 (d, 2H, H-2,6 pyridine, J = 4.5 Hz), 7.48 (bs, 2H, NH_2), 7.25 (d, 2H, H-3,5 pyridine, J = 4.5 Hz), 6.37 (s, 1H, H-5 thiophene), 3.98 (q, 2H, CH_2, J = 7.1 Hz), 0.92 (t, 3H, CH_3, J = 7.1 Hz); ^{13}C NMR (125 MHz, DMSO-d_6) δ: 165.89, 164.73, 150.28, 149.01 (2C), 146.10, 138.33, 124.07 (2C), 118.49, 107.60, 102.75, 59.33, 14.11; Anal. Calcd. For $C_{12}H_{12}N_2O_2S$: C, 58.05; H, 4.87; N, 11.28. Found: C, 58.22; H, 5.05; N, 11.41.

*5.1.2. 5-(Pyridin-4-yl)thieno[2,3-d]pyrimidin-4(3H)-one (**5**)*

As compound **4** (8.26 g, 33.3 mmol) was dissolved in DMF (90 ml) at 100 ^{o}C, formamidine acetate (24.26 g, 233.1 mmol) was added over 60 min and the mixture was stirred for 16 h. A yellow solid was precipitated, when cold water was added to the reaction mixture slowly. The precipitated solid was separated by filtration, washed with ether and allowed to be dry to give desired compound **5**, 5.66 g in 74% yield. Off-white solid; mp: 304-306 ^{o}C; IR (KBr, cm^{-1}): 3048, 1692, 1451, 1442, 1420,1359; ^{1}H NMR (400 MHz, DMSO-d_6) δ: 12.62 (bs, 1H, NH), 8.58 (d, 2H, H-2,6 pyridine, J = 4.5 Hz), 8.19 (s, 1H, H-2 thienopyrimidine), 7.77 (s, 1H, H-6

thienopyrimidine), 7.56 (d, 2H, H-3,5 pyridine, J = 4.5 Hz); ^{13}C NMR (125 MHz, DMSO-d_6) δ: 166.43, 157.73, 149.37 (2C), 146.60, 142.86, 136.19, 124.45 (2C), 123.61, 121.25; Anal. Calcd. For $C_{11}H_7N_3OS$: C, 57.63; H, 3.08; N, 18.33. Found: C, 57.51; H, 3.22; N, 18.50.

*5.1.3. 4-Chloro-5-(pyridin-4-yl)thieno[2,3-d]pyrimidine (**6**)*

Under the ice-bath condition, $POCl_3$ (8 ml) was added dropwise to a solution of compound **5** (920 mg, 4 mmol) and DIPEA (3 ml). After completion of the addition, the reaction mixture was warmed to room temperature and stirred for 30 min. Subsequently, the mixture was heated to 45 ^{o}C for 2 h. When the starting material was consumed, the reaction was cooled to room temperature. It was neutralized with saturated sodium bicarbonate solution and taken up in ethyl acetate and water. The organic layer was separated, dried over anhydrous Na_2SO_4, concentrated under vacuo and chromatographed on a flash silica gel column (EtOAc/petroleum ether = 1:1) to obtain the desired product **6**, 420 mg in 42% yield. Pale yellow solid; mp: 173-175 ^{o}C; IR (KBr, cm^{-1}): 3031, 1602, 1545, 1494; ^{1}H NMR (400 MHz, DMSO-d_6) δ: 9.01 (s, 1H, H-2 thienopyrimidine), 8.68 (d, 2H, H-2,6 pyridine, J = 4.4 Hz), 8.19 (s, 1H, H-6 thienopyrimidine), 7.56 (d, 2H, H-3,5 pyridine, J = 4.4 Hz); MS (*m/z*, %): 249 (M^+ +2, 33), 247 (M^+, 100), 212 (56); Anal. Calcd. For $C_{11}H_6ClN_3S$: C, 53.34; H, 2.44; N, 16.96. Found: C, 53.48; H, 2.58; N, 16.84.

*5.1.4. 5-Amino-1,3,4-thiadiazole-2-thiol (**9**)*

Thiosemicarbazide (**7**) (5 g, 54.94 mmol) and Na_2CO_3 (5.76 g, 54.94 mmol) were dissolved in dry ethanol and the mixture was heated to 60 ^{o}C for 30 min. Carbon disulfide (**8**) (8.35 g, 109.88 mmol) in dry ethanol was added dropwise and the resultant mixture was refluxed overnight. When the completion of the reaction was detected by TLC, the solvent was evaporated under reduced pressure. The residue was diluted through the addition of 100 ml water and then concentrated HCl solution was added carefully to obtain yellow precipitate known as 5-amino-1,3,4-thiadiazole-2-thiol or compound **9,** 6.2 g in 84% yield. Yellow solid; mp: 233-235 ^{o}C; IR (KBr, cm^{-1}): 3401, 3273, 1595, 1533, 1496; ^{1}H NMR (300 MHz, DMSO-d_6) δ: 13.11 (s, 1H, NH), 7.05 (s, 2H, NH_2); ^{13}C NMR (75 MHz, DMSO-d_6) δ: 180.93 (C-2, Thiadiazole), 161.48 (C-5, Thiadiazole); MS (*m/z*, %): 133 (M^+, 100), 74 (37.5), 57 (50); Anal. Calcd. For $C_2H_3N_3S_2$: C, 18.04; H, 2.27; N, 31.55. Found: C, 18.16; H, 2.36; N, 31.50.

*5.1.5. General procedure for synthesis of intermediates **10a-m***

Compound **9** (200 mg, 1.5 mmol) was dissolved in dry DCM and stirred at room temperature for 30 min. Then, appropriate phenyl isocyanate derivative (1.5 mmol) in dry DCM was added and the resulting yellowish mixture was allowed to stir under an argon atmosphere at room temperature overnight. The final white precipitate was kept in a vacuum oven for 2 h to give corresponding urea (**10a-m**). The product was used for the next step without any further purification.

*5.1.6. General procedure for synthesis of final compounds **11a-m***

A mixture of appropriate urea derivative (**10a-m**) (0.60 mmol) and KOH (33.6 mg, 0.60 mmol) in EtOH was stirred at 60^{o}C for 45 min, and then compound **6** (150 mg, 0.60 mmol) was added portion by portion over 5 min. The resulting mixture was refluxed overnight. The precipitated solid was filtered, washed with water and dried in a vacuum oven for 24 h to obtain the target compound (**11a-m**).

*5.1.6.1. 1-Phenyl-3-(5-((5-(pyridin-4-yl)thieno[2,3-d]pyrimidin-4-yl)thio)-1,3,4-thiadiazol-2-yl)urea (**11a**)*

Cream solid; yield: 63%; mp: 237-239 ^{o}C; IR (KBr, cm^{-1}): 3037, 1711, 1620, 1598, 1543, 1499; ^{1}H NMR (500 MHz, DMSO-d_6) δ: 9.12 (bs, 1H, NH urea), 8.94 (s, 1H, H-2 thienopyrimidine), 8.75 (d, 2H, H-2,6 pyridine, J = 4.5 Hz), 8.10 (s, 1H, H-6 thienopyrimidine), 7.64 (d, 2H, H-3,5 pyridine, J = 4.5 Hz), 7.48 (d, 2H, H-2,6 phenyl, J = 7.95 Hz), 7.33 (t, 2H, H-3,5 phenyl, J = 7.95 Hz), 7.07 (t, 1H, H-4 phenyl, J = 8.05 Hz); ^{13}C NMR (125 MHz, DMSO-d_6) δ: 167.67, 160.19, 152.39, 150.02 (2C), 142.94, 138.58, 132.43, 129.37 (2C), 128.72, 125.72, 125.46, 123.72, 119.50 (2C); Anal. Calcd. For $C_{20}H_{13}N_7OS_3$: C, 51.82; H, 2.83; N, 21.15. Found: C, 51.13; H, 2.73; N, 20.97.

*5.1.6.2. 1-(5-((5-(Pyridin-4-yl)thieno[2,3-d]pyrimidin-4-yl)thio)-1,3,4-thiadiazol-2-yl)-3-(m-tolyl)urea (**11b**)*

Cream solid; yield: 68%; mp: 231-236 ^{o}C; IR (KBr, cm^{-1}): 3381, 2917, 1712, 1634, 1600, 1495; ^{1}H NMR (500 MHz, DMSO-d_6) δ: 11.20 (bs, 1H, NH urea), 9.03 (bs, 1H, NH urea), 8.94 (s, 1H, H-2 thienopyrimidine), 8.74 (d, 2H, H-2,6 pyridine, J = 4.5 Hz), 8.09 (s, 1H, H-6 thienopyrimidine), 7.64 (d, 2H, H-3,5 pyridine, J = 4.5 Hz), 7.31 (s, 1H, H-2 m-tolyl), 7.25 (dd,

1H, H-6 m-tolyl, *J* = 8.2, 1.15 Hz), 7.19 (t, 1H, H-5 m-tolyl, *J* = 7.55 Hz), 6.87 (d, 1H, H-4 m-tolyl, *J* = 7.35 Hz), 2.28 (s, 3H, CH_3); ^{13}C NMR (75 MHz, DMSO-d_6) δ: 167.11, 163.96, 159.58, 151.85, 151.37, 149.50 (2C), 148.75, 142.41, 138.18, 137.99, 131.87, 128.70, 128.23, 125.12, 124.95 (2C), 123.89, 119.32, 116.02, 21.07; Anal. Calcd. For $C_{21}H_{15}N_7OS_3$: C, 52.81; H, 3.17; N, 20.53. Found: C, 52.64; H, 3.42; N, 20.31.

*5.1.6.3. 1-(3-Chlorophenyl)-3-(5-((5-(pyridin-4-yl)thieno[2,3-d]pyrimidin-4-yl)thio)-1,3,4-thiadiazol-2-yl)urea (**11c**)*

Cream solid; yield: 64%; mp: 236-239 ^{o}C; IR (KBr, cm^{-1}): 3375, 1731, 1596, 1498, 1454; ^{1}H NMR (500 MHz, DMSO-d_6) δ: 9.37 (bs, 1H, NH urea), 8.96 (s, 1H, H-2 thienopyrimidine), 8.75 (d, 2H, H-2,6 pyridine, *J* = 4.5 Hz), 8.10 (s, 1H, H-6 thienopyrimidine), 7.70 (s, 1H), 7.65 (d, 2H, H-3,5 pyridine, *J* = 4.5 Hz), 7.35 (d, 2H), 7.12 (d, 1H); ^{13}C NMR (125 MHz, DMSO-d_6) δ: 167.65, 164.47, 159.97, 152.35, 150.00 (2C), 149.47, 142.94, 140.24, 133.73, 132.39, 130.97, 128.76, 125.67, 125.45 (2C), 123.32, 118.86, 117.95; Anal. Calcd. For $C_{20}H_{12}ClN_7OS_3$: C, 48.24; H, 2.43; N, 19.69. Found: C, 48.42; H, 2.63; N, 19.52.

*5.1.6.4. 1-(5-((5-(Pyridin-4-yl)thieno[2,3-d]pyrimidin-4-yl)thio)-1,3,4-thiadiazol-2-yl)-3-(3-(trifluoromethyl)phenyl)urea (**11d**)*

Cream solid; yield: 67%; mp: 238-240 ^{o}C; IR (KBr, cm^{-1}): 3380, 1728, 1599, 1497, 1240, 1205, 1165, 1108, 1071; ^{1}H NMR (500 MHz, DMSO-d_6) δ: 11.54 (bs, 1H, NH urea), 9.58 (bs, 1H, NH urea), 8.95 (s, 1H, H-2 thienopyrimidine), 8.75 (d, 2H, H-2,6 pyridine, *J* = 4.5 Hz), 8.10 (s, 1H, H-6 thienopyrimidine), 7.99 (s, 1H, H-2 (3-trifluoromethyl)phenyl), 7.69 (d, 1H, H-6 (3-trifluoromethyl)phenyl, *J* = 7.25 Hz), 7.64 (d, 2H, H-3,5 pyridine, *J* = 4.5 Hz), 7.55 (t, 1H, H-5 (3-trifluoromethyl)phenyl, *J* = 7.95 Hz), 7.39 (d, 1H, H-4 (3-trifluoromethyl)phenyl, *J* = 7.25 Hz); ^{13}C NMR (125 MHz, DMSO-d_6) δ: 167.67, 152.42, 150.03 (2C), 142.93, 132.42, 130.54, 128.76 (q, $J_{C\text{-}F}$ = 2.31 Hz), 125.46 (2C), 123.16, 121.69 (q, $J_{C\text{-}F}$ = 7.4 Hz), 120.14 (q, $J_{C\text{-}F}$ = 16.15 Hz), 115.41 (q, $J_{C\text{-}F}$ = 4.81 Hz); MS (*m/z*, %): 531 (M^+, 0.6), 187 (50), 161 (100); Anal. Calcd. For $C_{21}H_{12}F_3N_7OS_3$: C, 47.45; H, 2.28; N, 18.45. Found: C, 47.60; H, 2.10; N, 18.73.

*5.1.6.5. 1-(3-Chloro-4-methylphenyl)-3-(5-((5-(pyridin-4-yl)thieno[2,3-d]pyrimidin-4-yl)thio)-1,3,4-thiadiazol-2-yl)urea (**11e**)*

Yellow solid; yield: 68%; mp: 231-133 ^{o}C; IR (KBr, cm^{-1}): 3257, 3183, 3041, 2976, 2920, 1606, 1498; ^{1}H NMR (500 MHz, DMSO-d_6) δ: 9.28 (bs, 1H, NH urea), 8.95 (s, 1H, H-2 thienopyrimidine), 8.75 (d, 2H, H-2,6 pyridine, J = 4.5 Hz), 8.10 (s, 1H, H-6 thienopyrimidine), 7.68 (s, 1H, H-2 (3-chloro-4-methyl)phenyl), 7.63 (d, 2H, H-3,5 pyridine, J = 4.5 Hz), 7.27 (s, 2H, H-5,6 (3-chloro-4-methyl)phenyl), 2.25 (s, 3H, CH_3); ^{13}C NMR (125 MHz, DMSO-d_6) δ: 167.67, 160.06, 152.38, 150.02 (2C), 142.94, 139.16, 137.86, 133.65, 132.42, 131.74, 131.57, 130.29, 128.75, 125.70, 125.46 (2C), 119.42, 118.24, 19.29; Anal. Calcd. For $C_{21}H_{14}ClN_7OS_3$: C, 49.26; H, 2.76; N, 19.15. Found: C, 49.10; H, 2.64; N, 18.97.

*5.1.6.6. 1-(4-Methoxyphenyl)-3-(5-((5-(pyridin-4-yl)thieno[2,3-d]pyrimidin-4-yl)thio)-1,3,4-thiadiazol-2-yl)urea (**11f**)*

White solid; yield: 65%; mp: 235-238 ^{o}C; IR (KBr, cm^{-1}): 3381, 3322, 2918, 1713, 1601, 1511; ^{1}H NMR (400 MHz, DMSO-d_6) δ: 11.24 (bs, 1H, NH urea), 9.00 (bs, 1H, NH urea), 8.97 (s, 1H, H-2 thienopyrimidine), 8.78 (d, 2H, H-2,6 pyridine, J = 4.5 Hz), 8.13 (s, 1H, H-6 thienopyrimidine), 7.67 (d, 2H, H-3,5 pyridine, J = 4.5 Hz), 7.40 (d, 2H, H-2,6 methoxyphenyl, J = 8.8 Hz), 6.93 (d, 2H, H-3,5 methoxyphenyl, J = 9.2 Hz), 3.74 (s, 3H, OCH_3); Anal. Calcd. For $C_{21}H_{15}N_7O_2S_3$: C, 51.10; H, 3.06; N, 19.86. Found: C, 50.93; H, 2.81; N, 19.68.

*5.1.6.7. 1-(5-((5-(Pyridin-4-yl)thieno[2,3-d]pyrimidin-4-yl)thio)-1,3,4-thiadiazol-2-yl)-3-(p-tolyl)urea (**11g**)*

Cream solid; yield: 67%; mp: 234-237 ^{o}C; IR (KBr, cm^{-1}): 3396, 1707, 1597, 1420, 1315; ^{1}H NMR (500 MHz, DMSO-d_6) δ: 11.20 (bs, 1H, NH urea), 9.04 (bs, 1H, NH urea), 8.93 (s, 1H, H-2 thienopyrimidine), 8.75 (d, 2H, H-2,6 pyridine, J = 4.5 Hz), 8.09 (s, 1H, H-6 thienopyrimidine), 7.63 (d, 2H, H-3,5 pyridine, J = 4.5 Hz), 7.35 (d, 2H, H-2,6 p-tolyl, J = 8.2 Hz), 7.12 (d, 2H, H-3,5 p-tolyl, J = 8.2 Hz), 2.24 (s, 3H, CH_3); ^{13}C NMR (125 MHz, DMSO-d_6) δ: 167.67, 160.22, 152.39, 150.02 (2C), 142.95, 136.02, 132.74, 132.43, 129.76 (2C), 129.56, 128.71, 125.72, 125.45 (2C), 119.55 (2C), 20.81; Anal. Calcd. For $C_{21}H_{15}N_7OS_3$: C, 52.81; H, 3.17; N, 20.53. Found: C, 52.99; H, 3.42; N, 20.43.

*5.1.6.8. 1-(4-Fluorophenyl)-3-(5-((5-(pyridin-4-yl)thieno[2,3-d]pyrimidin-4-yl)thio)-1,3,4-thiadiazol-2-yl)urea (**11h**)*

White solid; yield: 60%; mp: 235-237 ^{o}C; IR (KBr, cm^{-1}): 3393, 1717, 1599, 1509, 1459; ^{1}H NMR (500 MHz, DMSO-d_6) δ: 11.25 (bs, 1H, NH urea), 9.19 (bs, 1H, NH urea), 8.93 (s, 1H, H-2 thienopyrimidine), 8.75 (d, 2H, H-2,6 pyridine, J = 4.5 Hz), 8.09 (s, 1H, H-6 thienopyrimidine), 7.63 (d, 2H, H-3,5 pyridine, J = 4.5 Hz), 7.48-7.50 (m, 2H, H-2,6 fluorophenyl), 7.15 (t, 2H, H-3,5 fluorophenyl, J = 8.7 Hz); ^{13}C NMR (75 MHz, DMSO-d_6) δ: 167.14, 164.42, 159.52, 152.33, 151.89, 149.51 (2C), 148.80, 142.43, 139.29, 131.89, 130.02, 129.77, 129.35, 128.26, 125.82, 125.15, 124.95 (2C), 122.59, 119.30 (d, 2C, $J_{C\text{-}F}$ = 7.86 Hz), 114.87 (d, 2C, $J_{C\text{-}F}$ = 14.41 Hz); MS (*m/z*, %): 481 (M^+, 3), 137 (67), 111 (100), 83 (42), 57 (30); Anal. Calcd. For $C_{20}H_{12}FN_7OS_3$: C, 49.89; H, 2.51; N, 20.36. Found: C, 50.10; H, 2.70; N, 20.18.

*5.1.6.9. 1-(3,4-Dichlorophenyl)-3-(5-((5-(pyridin-4-yl)thieno[2,3-d]pyrimidin-4-yl)thio)-1,3,4-thiadiazol-2-yl)urea (**11i**)*

Cream solid; yield: 64%; mp: 233-238 ^{o}C; IR (KBr, cm^{-1}): 3361, 1719, 1599, 1585, 1531, 1494; ^{1}H NMR (500 MHz, DMSO-d_6) δ: 11.55 (bs, 1H, NH urea), 9.44 (bs, 1H, NH urea), 8.95 (s, 1H, H-2 thienopyrimidine), 8.74 (d, 2H, H-2,6 pyridine, J = 4.5 Hz), 8.10 (s, 1H, H-6 thienopyrimidine), 7.87 (d, 1H, H-2 dichlorophenyl, J = 2 Hz), 7.63 (d, 2H, H-3,5 pyridine, J = 4.5 Hz), 7.55 (d, 1H, H-5 dichlorophenyl, J = 8.65 Hz), 7.43 (dd, 1H, H-6 dichlorophenyl, J = 8.85, 1.85 Hz); ^{13}C NMR (75 MHz, DMSO-d_6) δ: 167.13, 164.03, 159.36, 152.04, 151.82, 149.47 (2C), 148.97, 142.43, 138.49, 131.84, 131.08, 130.61, 128.29, 125.12, 124.94 (2C), 124.55, 120.11, 119.08; MS (*m/z*, %): 531 (M^+, 0.2), 233 (17), 191 (4), 189 (24), 187 (40), 165 (10), 163 (60), 161 (100); Anal. Calcd. For $C_{20}H_{11}Cl_2N_7OS_3$: C, 45.12; H, 2.08; N, 18.42. Found: C, 44.84; H, 2.87; N, 18.26.

*5.1.6.10. 1-(4-Chlorophenyl)-3-(5-((5-(pyridin-4-yl)thieno[2,3-d]pyrimidin-4-yl)thio)-1,3,4-thiadiazol-2-yl)urea (**11j**)*

White solid; yield: 67%; mp: 236-238 ^{o}C; IR (KBr, cm^{-1}): 3389, 1720, 1597, 1493, 1076; ^{1}H NMR (500 MHz, DMSO-d_6) δ: 11.39 (bs, 1H, NH urea), 9.36 (bs, 1H, NH urea), 8.94 (s, 1H, H-2 thienopyrimidine), 8.75 (d, 2H, H-2,6 pyridine, J = 4.5 Hz), 8.09 (s, 1H, H-6 thienopyrimidine), 7.63 (d, 2H, H-3,5 pyridine, J = 4.5 Hz), 7.51 (d, 2H, H-2,6 chlorophenyl, J = 7.6 Hz), 7.37 (d, 2H, H-3,5 chlorophenyl, J = 7.8 Hz); ^{13}C NMR (125 MHz, DMSO-d_6) δ:

167.67, 164.50, 160.11, 152.37, 150.01 (2C), 142.93, 137.70, 132.42, 129.21 (2C), 129.03, 128.72, 127.32, 125.70, 125.44 (2C), 121.03 (2C), 120.27; Anal. Calcd. For $C_{20}H_{12}ClN_7OS_3$: C, 48.24; H, 2.43; N, 19.69. Found: C, 48.07; H, 2.66; N, 19.42.

*5.1.6.11. 1-(4-Chloro-3-(trifluoromethyl)phenyl)-3-(5-((5-(pyridin-4-yl)thieno[2,3-d]pyrimidin-4-yl)thio)-1,3,4-thiadiazol-2-yl)urea (**11k**)*

White solid; yield: 67%; mp: 239-240 ^{o}C; IR (KBr, cm^{-1}): 3389, 1720, 1597, 1546, 1493, 1458, 1340, 1310, 1093, 1076; ^{1}H NMR (300 MHz, DMSO-d_6) δ: 11.89 (bs, 1H, NH urea), 9.99 (s, 1H, NH urea), 8.92 (s, 1H, H-2 thienopyrimidine), 8.74 (d, 2H, H-2,6 pyridine, J = 4.2 Hz), 8.07 (s, 2H), 7.75 (d, 1H, J = 10.1 Hz), 7.62 (d, 3H); ^{13}C NMR (75 MHz, DMSO-d_6) δ: 167.14, 164.40, 159.45, 152.50, 151.87, 149.51 (2C), 148.86, 142.42, 138.11, 132.08, 131.87, 128.29, 125.51 (q, $J_{C\text{-}F}$ = 158.85 Hz), 125.13, 124.95 (2C), 123.72, 123.63, 117.50 (q, $J_{C\text{-}F}$ = 5.49 Hz); MS (*m/z*, %): 565 (M^+, 0.5), 456 (18), 244 (24), 223 (23), 221 (69), 197 (30), 195 (100); Anal. Calcd. For $C_{21}H_{11}ClF_3N_7OS_3$: C, 44.56; H, 1.96; N, 17.32. Found: C, 44.74; H, 2.13; N, 17.51.

*5.1.6.12. 1-(3-Methoxyphenyl)-3-(5-((5-(pyridin-4-yl)thieno[2,3-d]pyrimidin-4-yl)thio)-1,3,4-thiadiazol-2-yl)urea (**11l**)*

White solid; yield: 62%; mp: 238-240 ^{o}C; IR (KBr, cm^{-1}): 3373, 1725, 1597, 1545, 1494, 1300, 1237, 1216, 1163; ^{1}H NMR (500 MHz, DMSO-d_6) δ: 11.20 (bs, 1H, NH urea), 9.14 (bs, 1H, NH urea), 8.94 (s, 1H, H-2 thienopyrimidine), 8.75 (d, 2H, H-2,6 pyridine, J = 4.5 Hz), 8.09 (s, 1H, H-6 thienopyrimidine), 7.64 (d, 2H, H-3,5 pyridine, J = 4.5 Hz), 7.22 (t, 1H, H-5 methoxyphenyl, J = 8.2 Hz), 7.14 (s, 1H, H-2 methoxyphenyl), 6.99 (dd, 1H, H-6 methoxyphenyl, J = 7.2, 1.25 Hz), 6.63 (dd, 1H, H-4 methoxyphenyl, J = 8.2, 2.1 Hz), 3.73 (s, 3H, OCH_3); ^{13}C NMR (125 MHz, DMSO-d_6) δ: 167.68, 160.21, 160.16, 152.39, 150.01 (2C), 142.94, 139.78, 132.43, 130.19, 128.71, 125.71, 125.45 (2C), 111.75, 109.17, 105.33, 55.55; Anal. Calcd. For $C_{21}H_{15}N_7O_2S_3$: C, 51.10; H, 3.06; N, 19.86. Found: C, 51.27; H, 3.24; N, 19.69.

*5.1.6.13. 1-(3-Fluorophenyl)-3-(5-((5-(pyridin-4-yl)thieno[2,3-d]pyrimidin-4-yl)thio)-1,3,4-thiadiazol-2-yl)urea (**11m**)*

Cream solid; yield: 65%; mp: 234-236 ^{o}C; IR (KBr, cm^{-1}): 3390, 1716, 1599, 1547; ^{1}H NMR (300 MHz, DMSO-d_6) δ: 11.42 (bs, 1H, NH urea), 9.38 (s, 1H, NH urea), 8.90 (s, 1H, H-2

thienopyrimidine), 8.73 (d, 2H, H-2,6 pyridine, J = 4.5 Hz), 8.05 (s, 1H, H-6 thienopyrimidine), 7.60 (d, 2H, H-3,5 pyridine, J = 4.5 Hz), 7.45 (d, 1H, H-6 fluorophenyl, J = 10.95 Hz), 7.28-7.33 (m, 1H, H-5 fluorophenyl), 7.20 (d, 1H, H-2 fluorophenyl, J = 7.11 Hz), 6.84 (bs, 1H, H-4 fluorophenyl); ^{13}C NMR (75 MHz, DMSO-d_6) δ: 167.13, 163.93, 161.7 (d, $J_{C\text{-}F}$ = 240.74 Hz), 159.47, 152.04, 151.83, 151.74, 149.50 (2C), 148.99, 142.45, 140.01 (d, $J_{C\text{-}F}$ = 10.85 Hz), 131.87, 130.46 (d, $J_{C\text{-}F}$ = 9.24 Hz), 128.78, 128.28, 124.97 (2C), 114.70, 109.49 (d, $J_{C\text{-}F}$ = 21.06 Hz), 105.69 (d, $J_{C\text{-}F}$ = 26.24 Hz); Anal. Calcd. For $C_{20}H_{12}FN_7OS_3$: C, 49.89; H, 2.51; N, 20.36. Found: C, 50.01; H, 2.74; N, 20.18.

5.2. MTT assay

Cytotoxicity of synthesized target compounds (**11a-m**) was examined with MTT assay. For this purpose, concerning similar studies, four appropriate cancer cell lines (PC3, HepG2, T47D, and HUVEC) were selected provided by the National Cell Bank of Iran (Pastor Institute, Tehran, Iran). Contents of each well in a 96-well microtiter plate included 200 µl of complete medium containing 8000 cells, incubated at 37 ^{o}C in a humidified 5% CO_2 incubator overnight. Cells were exposed to various concentrations of test compounds prepared earlier (in DMSO) and further incubated at 37 ^{o}C for 48 h. After incubation, the solution containing 5% MTT was added to all wells and incubated for another 4 h. The absorbance was measured with a microplate reader (Bio-Rad microplate reader, Model 680) at a test wavelength of 570 nm. The absorbance measured is directly proportional to the percentage of live cells. A simple calculation known as half-maximal inhibitory concentration (IC_{50}) was used to gauge whether target compounds are effective or not. As a consequence, particular curves indicating cell survival percentage versus different concentrations of the compounds were drawn and analyzed. Herein, sorafenib and 0.1% DMSO were regarded as positive and negative controls, respectively.

5.3. Analysis of cellular apoptosis

Annexin V-FITC/propidium iodide dual staining assay was implemented to analyze the induction of apoptosis by **11h** and **11i** (tested at IC_{50}). PC3 cells were seeded into 6-well plates and incubated overnight at 37 ^{o}C under 5% CO2. Cells were exposed to the IC_{50} of target compounds and then incubated for 48 h. Treated cells were trypsinized, washed with PBS twice, and centrifuged at 1200 rpm. After that, 500 ml of binding buffer and 5 ml of Annexin V-FITC and PI were added to suspended cells. Finally, to examine the cell apoptosis with the assistance

of flow cytometry (FACS Calibur Bectone-Dickinson), suspended cells were incubated at room temperature in darkness for 5-15 min. The potential proapoptotic activity of **11i** was surveyed in a similar way against the HUVEC cell line. In these experiments, sorafenib was utilized as the positive control [30].

5.4. Cell cycle analysis

Through flow cytometry analysis, propidium iodide (PI) staining assay was implemented as a challenge to explore the cell cycle distribution in PC3 cells. PI attaches to the DNA molecule and emits a fluorescent, the intensity of which is directly proportional to the DNA content. The cells were exposed to IC_{50} of test compounds (**11h** and **11i**), after 48 h, the treated cells were trypsinized, washed with PBS, and centrifuged at 1200 rpm for 5 min. As soon as the incubation with PBS was carried out, prepared PC3 cells were fixed with 70% cold ethanol (-20 ^{o}C). The fixed cells were washed with PBS. After rinsing, in an orderly fashion, they were treated with RNase A (0.1 mg/ml), incubated for half an hour, and exposed to 50 mg/ml of PI, continuously incubated for 15 min more. To calculate the cell cycle distribution, the familiar equipment, Novocyte flow cytometer (ACEA Biosciences) was employed, and the data were analyzed by NovoExpress 1.1.0 software. All the experiments were performed on three samples in parallel. The cell cycle analysis of HUVEC was performed similarly.

5.5. Chick chorioallantoic membrane (CAM) assay

Since the allantois of the chick embryo appears at about 3.5 days of incubation, the corresponding eggs were incubated (37.5 ^{o}C, relative humidity: 55-65%). To decrease the risk of infection, the particular regions of the egg, e.g., the front side of the embryo were cleaned and sterilized with 70% EtOH. On the 6th incubation day, a false air sac was created directly over the CAM, permitting its detachment from the shell membrane. The procedure was continued through a square incision over the CAM. The prepared window in a square form (1×1 cm), was covered by a flexible film and then transported to the incubator. On the 8th incubation day, the particular paper discs (Whatman) were coated with target agents and placed in the central area of the corresponding window. The surface of CAM was visually evaluated on the 12th incubation day using the stereomicroscope. We decided to use the number and the length of capillary blood vessels as the index of anti-angiogenic activity. Consequently, the prepared images were analyzed by the advantageous software, Image J [31].

5.6. Western blot analysis

When exposed to IC_{50} of corresponding compounds, **11i** and sorafenib, PC3 cells were incubated for 24, 48, and 72 h. PC3 cells were thawed in a 100 ml lysis buffer and immediately lysed. Then, they were centrifuged at 1200 rpm at 4 ^{o}C for 10 min. The obtained total proteins were loaded and electrophoresed on 12% SDS-PAGE and transferred to a nitrocellulose membrane (0.45 mm) for 1.5 h at 100 V and blocked with 5% blocking buffer. The next step in the western blotting was the incubation of prepared antibodies at 4 ^{o}C for 12 h. The housekeeping protein utilized in this procedure was beta-actin. Immunoblots were uncovered using the enhanced chemiluminescence (ECL) method.

5.7. Molecular docking study

The analysis of data prepared by Western blotting has challenged us to explore the best poses and interactions of compound **11i** in the active site of the receptor and for this purpose, the AutoDock 4.2 program was implemented. The crystallographic structure of the VEGFR-2 receptor in complex with ligand sorafenib (3WZE) was taken from PDB. To prepare 2D structures, MarvinSketch 15.10.12 was utilized and using Chem3D ultra 8.0, the corresponding structures were minimized and converted to pdb format. The next step involved the preparation of the corresponding macromolecule; VEGFR-2, so that extra molecules of the protein were removed by the discovery studio software and subsequently polar hydrogens and electric charges added by AutoDockTools version 1.5.6. All maps were provided with 0.375 Å spacing between grid points and through the selection of appropriate coordinates 81 Å (x), 61 Å (y), and 64 Å (z), the proper location of the grid box was determined [32]. Discovery Studio Visualizer (Ver. 17.2) and Pymol (Ver. 1.level) were used to visualize possible interactions between the receptor and the ligand. Finally, to validate the docking protocol, the RMSD was calculated (0.46 Å) which was demonstrating a successfully docked procedure (Fig. 14).

Acknowledgement

This work was supported and funded by Tehran University of Medical Sciences and Health Services Grant no. 98-3-104-45990; and National Institute for Medical Research Development Grant no. 962567.

References

1. J. Ferlay, M. Colombet, I. Soerjomataram, C. Mathers, D.M. Parkin, M. Piñeros, A. Znaor, F. Bray, Estimating the global cancer incidence and mortality in 2018: GLOBOCAN sources and methods, Int. J. Cancer. 144 (2019) 1941-53. https://doi.org/10.1002/ijc.31937.
2. F. Musumeci, M. Radi, C. Brullo, S. Schenone, Vascular endothelial growth factor (VEGF) receptors: drugs and new inhibitors, J. Med. Chem. 55 (2012) 10797-10822. https://doi.org/10.1021/jm301085w.
3. N. Ferrara, H.P. Gerber, J. LeCouter, The biology of VEGF and its receptors, Nat. Med. 9 (2003) 669-676. https://doi.org/10.1038/nm0603-669.
4. L. Zhang, Y. Shan, X. Ji, M. Zhu, C. Li, Y. Sun, R. Si, X. Pan, J. Wang, W. Ma, B. Dai, Discovery and evaluation of triple inhibitors of VEGFR-2, TIE-2 and EphB4 as anti-angiogenic and anti-cancer agents, Oncotarget. 8 (2017) 104745-104760. https://doi.org/10.18632/oncotarget.20065.
5. Y. Zhao, F. Liu, G. He, K. Li, C. Zhu, W. Yu, C. Zhang, M. Xie, J. Lin, J. Zhang, Y. Jin, Discovery of arylamide-5-anilinoquinazoline-8-nitro derivatives as VEGFR-2 kinase inhibitors: synthesis, in vitro biological evaluation and molecular docking. Bioorg. Med. Chem. Let. 29 (2019) 126711-126711. https://doi.org/10.1016/j.bmcl.2019.126711.
6. H. Fan, D. Wei, K. Zheng, X. Qin, L. Yang, Y. Yang, Y. Duan, Y. Xu, L. Hu, Discovery of Dioxino [2,3-f] quinazoline derivative VEGFR-2 inhibitors exerting significant antipro-liferative activity in HUVECs and mice, Eur. J. Med.l Chem. 175 (2019) 349-56. https://doi.org/10.1016/j.ejmech.2019.04.015.
7. A. Ghith, K.M. Youssef, N.S. Ismail, K.A. Abouzid, Design, synthesis and molecular modeling study of certain VEGFR-2 inhibitors based on thienopyrimidne scaffold as cancer targeting agents, Bioorg. Chem. 83 (2019) 111-128. https://doi.org/ 10.1016/j.bioorg.2018.10.008.
8. M.A. Aziz, R.A. Serya, D.S. Lasheen, A.K. Abdel-Aziz, A. Esmat, A.M. Mansour, A.N. Singab, K.A. Abouzid, Discovery of potent VEGFR-2 inhibitors based on furopyrimidine and thienopyrimidne scaffolds as cancer targeting agents, Sci. Rep. 6 (2016) 24460-24480. https://doi.org/ 10.1038/srep24460.
9. H.K. Mahmoud, T.A. Farghaly, H.G. Abdulwahab, N.T. Al-Qurashi, M.R. Shaaban. Novel 2-Indolinone Thiazole Hybrids as Sunitinib Analogues: Design, Synthesis, and Potent VEGFR-2 Inhibition with Potential Anti-Renal Cancer Activity, Eur. J. Med. Chem. 208 (2020) 112752-112766. https://doi.org/10.1016/j.ejmech.2020.112752.
10. W.M. Eldehna, M. Fares, H.S. Ibrahim, M.H. Aly, S. Zada, M.M. Ali, S.M. Abou-Seri, H.A. Abdel-Aziz, D.A. Abou El Ella, Indoline ureas as potential anti-hepatocellular carcinoma agents targeting VEGFR-2: Synthesis, in vitro biological evaluation and molecular docking, Eur. J. Med. Chem. 100 (2015) 89-97.
11. Wang C, Gao H, Dong J, Zhang Y, Su P, Shi Y, Zhang J. Biphenyl derivatives incorporating urea unit as novel VEGFR-2 inhibitors: design, synthesis and biological evaluation, Bioorg. Med. Chem. 22 (2014) 277-284. https://doi.org/10.1016/j.bmc.2013.11.027.
12. Y. Shan, R. Si, J. Wang, Q. Zhang, J. Li, Y. Ma, J. Zhang, Discovery of novel anti-angiogenesis agents. Part 11: Development of PROTACs based on active molecules with potency of promoting vascular normalization, Eur. J. Med. Chem. 205 (2020) 112654-112667. https://doi.org/10.1016/j.ejmech.2020.112654.
13. W. Sun, S. Hu, S. Fang, H. Yan, Design, synthesis and biological evaluation of pyrimidine-based derivatives as VEGFR-2 tyrosine kinase inhibitors, Bioorg. Chem. https://doi.org/10.1016/j.bioorg.2018.04.005.
14. J. Li, W. Gu, X. Bi, H. Li, C. Liao, C. Liu, W. Huang, H. Qian, Design, synthesis, and biological evaluation of thieno [2, 3-d] pyrimidine derivatives as novel dual c-Met and VEGFR-2 kinase inhibitors, Bioorg. Med. Chem. 25 (2017) 6674-6679. https://doi.org/ 10.1016/j.bmc.2017.11.010.
15. E.M. Ali, M.S. Abdel-Maksoud, C.H. Oh, Thieno [2, 3-d] pyrimidine as a promising scaffold in medicinal chemistry: Recent advances, Bioorg. Med. Chem. 27 (2019) 1159-1194. https://doi.org/ 10.1016/j.bmc.2019.02.044.

16. L. Zhang, Y. Shan, C. Li, Y. Sun, P. Su, J. Wang, L. Li, X. Pan, J. Zhang, Discovery of novel anti-angiogenesis agents. Part 6: Multi-targeted RTK inhibitors, Eur. J. Med. Chem. 127 (2017) 275-285. https://doi.org/10.1016/j.bmc.2017.11.010.
17. H.M. Patel, P. Bari, R. Karpoormath, M. Noolvi, N. Thapliyal, S. Surana, P. Jain, Design and synthesis of VEGFR-2 tyrosine kinase inhibitors as potential anticancer agents by virtual based screening, RSC Adv. 70 (2015) 56724-56771. https://doi.org/10.1039/C5RA05277G.
18. X. Pan, L. Liang, R.U. Si, J. Wang, Q. Zhang, H. Zhou, L. Zhang, J. Zhang, Discovery of novel anti-angiogenesis agents. Part 10: Multi-target inhibitors of VEGFR-2, Tie-2 and EphB4 incorporated with 1, 2, 3-triazol, Eur. J. Med. Chem. 163 (2019) 1-9. https://doi.org/10.1016/j.ejmech.2018.11.042.
19. C. Li, Y. Shan, Y. Sun, R. Si, L. Liang, X. Pan, B. Wang, J. Zhang, Discovery of novel anti-angiogenesis agents. Part 7: Multitarget inhibitors of VEGFR-2, TIE-2 and EphB4, Eur. J. Med. Chem. 141 (2017) 506-518. https://doi.org/10.1016/j.ejmech.2017.10.030.
20. Y. Shan, H. Gao, X. Shao, J. Wang, X. Pan, J. Zhang, Discovery of novel VEGFR-2 inhibitors. Part 5: Exploration of diverse hinge-binding fragments via core-refining approach, Eur. J. Med. Chem. 103(2015) 80-90. https://doi.org/10.1016/j.ejmech.2015.08.045.
21. E.F. Abdelhaleem, M.K. Abdelhameid, A.E. Kassab, M.M. Kandeel, Design and synthesis of thienopyrimidine urea derivatives with potential cytotoxic and pro-apoptotic activity against breast cancer cell line MCF-7, Eur. J. Med. Chem. 143 (2018) 1807-1825. https://doi.org/10.1016/j.ejmech.2017.10.075.
22. S. Zhang, Z. Cao, H. Tian, G. Shen, Y. Ma, H. Xie, Y. Liu, C. Zhao, S. Deng, Y. Yang, R. Zheng, SKLB1002, a novel potent inhibitor of VEGF receptor 2 signaling, inhibits angiogenesis and tumor growth in vivo, Clin. Cancer Res. 17 (2011) 4439-4450. https://doi.org/10.1158/1078-0432.CCR-10-3109.
23. Q.Y. Zhang, S.Y. Tao, C. Lu, J.J. Li, X.M. Li, J. Yao, Q. Jiang, B. Yan, SKLB1002, a potent inhibitor of VEGF receptor 2 signaling, inhibits endothelial angiogenic function in vitro and ocular angiogenesis in vivo, Mol. Med. Rep. 21 (2020) 2571-2579. https://doi.org/10.3892/mmr.2020.11056.
24. K. Gewald, E. Schinke, H. Böttcher, Heterocyclen aus CH-aciden Nitrilen, VIII. 2-Amino-thiophene aus methylenaktiven Nitrilen, Carbonylverbindungen und Schwefel, Chem. Ber. 99 (1966) 94-100. https://doi.org/10.1002/cber.19660990116.
25. K. Gewald, G. Neumann, Heterocyclen aus CH-aciden Nitrilen, XIV. 2-Amino-thionaphthene, Chem. Ber. 101 (1968) 1933-1939. https://doi.org/10.1002/cber.19681010607.
26. E. Roberts, D.A.F. Cossigny, G.M.Y. Quan, The Role of Vascular Endothelial Growth Factor in Metastatic Prostate Cancer to the Skeleton, Prostate Cancer. (2013). https://doi.org/10.1155/2013/418340.
27. J. Rak, C. Milsom, L. May, P. Klement, J. Yu, Tissue factor in cancer and angiogenesis: The molecular link between genetic tumor progression, tumor neovascularization, and cancer coagulopathy, Semin. Thromb. Hemost. 32 (2006) 54-70. https://doi.org/10.1055/s-2006-933341.
28. K. Okamoto, M. Ikemori-Kawada, A. Jestel, K. Von König, Y. Funahashi, T. Matsushima, A. Tsuruoka, A. Inoue, J. Matsui, Distinct binding mode of multikinase inhibitor lenvatinib revealed by biochemical characterization, ACS Med. Chem. Lett. 6 (2015) 89-94. https://doi.org/10.1021/ml500394m.
29. F. Meng, Molecular Dynamics Simulation of VEGFR2 with Sorafenib and Other Urea-Substituted Aryloxy Compounds, J. Theor. Chem. (2013). https://doi.org/10.1155/2013/739574.
30. M. Toolabi, S. Moghimi, T.O. Bakhshaiesh, S. Salarinejad, A. Aghcheli, Z. Hasanvand, E. Nazeri, A. Khalaj, R. Esmaeili, A. Foroumadi, 6-Cinnamoyl-4-arylaminothienopyrimidines as highly potent cytotoxic agents: Design, synthesis and structure-activity relationship studies, Eur. J. Med. Chem. 185 (2020) 111786-111793. https://doi.org/10.1016/j.ejmech.2019.111786.
31. A.M. Cimpean, D. Ribatti, M. Raica, The chick embryo chorioallantoic membrane as a model to study tumor metastasis, Angiogenesis. 11 (2008) 311-319. https://doi.org/10.1007/s10456-008-9117-1.
32. J. Bao, N. Zhou, K. Luo, W. Zhang, X. Li, C. Wu, J. Bao, In silico discovery of potential VEGFR-2 inhibitors from natural derivatives for anti-angiogenesis therapy, Int. J. Mol. Sci. 15 (2014) 15994-6011, https://doi.org/10.3390/ijms150915994.

Captions:

Table 1. *In vitro* anti-proliferative effects (IC_{50}, μM) of compounds **11a-m** against PC3, HepG2, T47D and HUVEC cell lines.

Table 2. *In vitro* cytotoxic effects (IC_{50}, μM) of compound **11i** against Hu02 cell line.

Figure 1. Diaryl urea containing anticancer agents in clinical use or in clinical trials.

Figure 2. Design strategy of final compounds **11a-m**.

Figure 3. Flow cytometry analysis of PC3 cells treated with compounds **11h** and **11i**. (a) Nontreated cells as negative control group; (b) treated with sorafenib as positive control at its IC_{50}; (c) treated with **11h** at its IC_{50}; (d) treated with **11i** at its IC_{50}; (e) treated with dimethyl sulfoxide as solvent. Early apoptotic cells (Annexin V-positive, propidium iodide-negative) appear in the lower right quadrant and late apoptotic cells (positive for both markers) in the upper right quadrant.

Figure 4. Flow cytometry analysis of HUVEC cells treated with compound **11i**. (a) Nontreated cells as negative control group; (b) treated with sorafenib as positive control at its IC50; (c) treated with **11i** at its IC50; (d) treated with dimethyl sulfoxide as solvent. Early apoptotic cells (Annexin V-positive, propidium iodide-negative) appear in the lower right quadrant and late apoptotic cells (positive for both markers) in the upper right quadrant.

Figure 5. Effect of compounds **11h** and **11i** on the cell cycle distribution of PC3 cells by flow cytometry analysis. (a) Non-treated cells as the control group; (b) treated with **11h** at its IC_{50}; (c) treated with **11i** at its IC_{50}; (d) treated with sorafenib at its IC_{50}.

Figure 6. Quantitative measurement of the cell cycle analysis.

Figure 7. The amount of apoptosis mediated by **11h**, **11i**, and sorafenib versus the cell population arrested in the subG1-phase. The graph was presented by separated symbols, trying to make a logical connection between the dependent variables.

Figure 8. Effect of compound **11i** on the cell cycle distribution of HUVEC cells by flow cytometry analysis. (a) Non-treated cells as the control group; (b) treated with **11i** at its IC_{50}; (c) treated with sorafenib at its IC_{50}.

Figure 9. Screening compounds by chick chorioallantoic membrane (CAM) assay. (a) Negative control; (b) sorafenib; (c) **11i**.

Fig. 10. a) Quantification of the effects of **11b**, **11h**, **11i**, **11j**, and **11m** on the number of CAM blood vessels. The bars show the mean ± SD (n=5). Statistical significance: **P < 0.01. b) Quantification of the effects of **11b**, **11h**, **11i**, **11j**, and **11m** on the length of CAM blood vessels. The bars show the mean ± SD (n=5). Statistical significance: **P < 0.01, ***P <0.001. **11i** concentration: 3.6 μM; sorafenib concentration: 15.5 μM.

Figure 11. Western blot analysis of **11i** and sorafenib on the VEGFR-2 phosphorylation in the PC3 cell line after 24, 48, and 72 h.

Figure 12. Expression of VEGFR-2 and p-VEGFR-2 in PC3 cells treated with different concentrations of **11i** for 48 h. Control: treated with no drug; **11i**-L: treated with 2.4 μM **11i**; **11i**-N: treated with 3.6 μM **11i**; **11i**-H: treated with 5.4 μM **11i**.

Figure 13. a) 2D illustration of compound **11i** and the corresponding interactions with residues in the active site of VEGFR-2; b) 3D illustration of compound **11i** and the corresponding interactions with residues in the active site of VEGFR-2.

Figure 14. Superimposed representation of redocking lowest energy poses into the co-crystalized ligand sorafenib over 3WZE.

Scheme 1. Reagents and conditions: a) morpholine, reflux, 14 h, 70%; b) formamidine acetate, DMF, 100 ^{o}C, 16 h, 74%; c) $POCl_3$, DIPEA, 45 ^{o}C, 42%; d) sodium carbonate, dry EtOH, reflux, 8 h, 84%; e) various substituted phenyl isocyanate, dry DCM, rt, 24 h, 45-55%; f) KOH/EtOH, reflux, 6h, 60-68%.

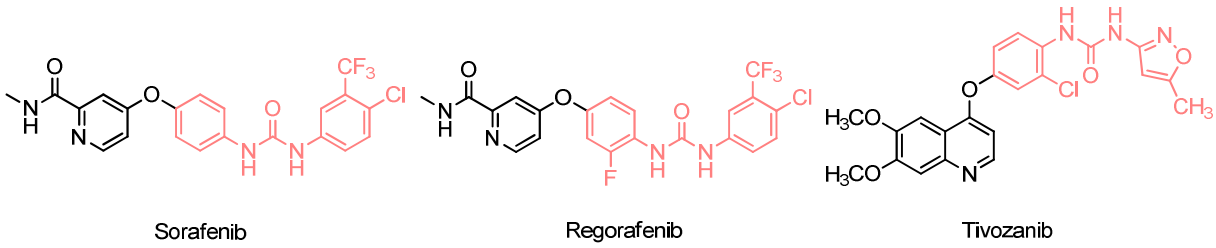

Fig. 1. Approved VEGFR-2 inhibitors containing diaryl ureas

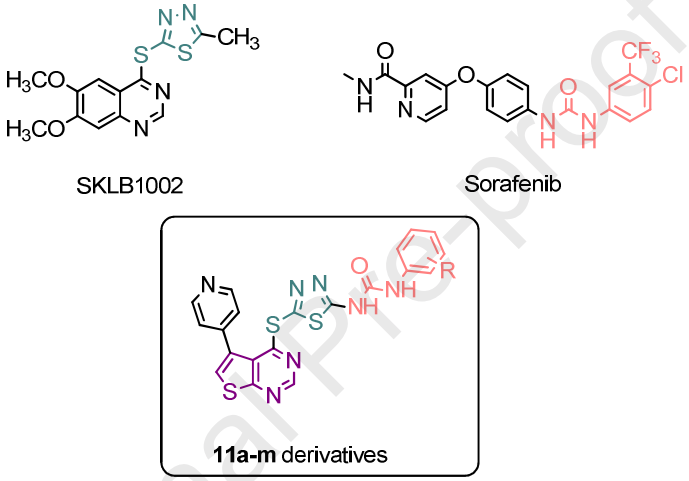

Fig. 2. Design strategy of final compounds **11a-m**.

Table 1: *In vitro* anti-proliferative effects (IC_{50}, μM) of compounds 11a-m against PC3, HepG2, T47D and HUVEC cell lines[a].

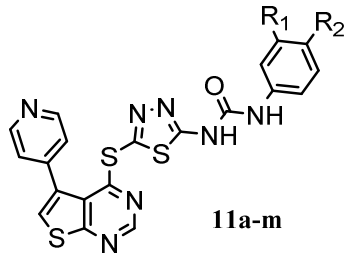

11a-m

Compound	R_1	R_2	PC3	HepG2	T47D	HUVEC
11a	H	H	**5.7** ± 0.8	**19.4** ± 0.5	23.3 ± 0.5	19.3 ± 0.5
11b	CH_3	H	**5.2** ± 0.8	**20.7** ± 0.4	27.2 ± 0.4	12.2 ± 0.5
11c	Cl	H	**8.0** ± 0.7	**22.9** ± 0.4	43.9 ± 0.2	21.0 ± 0.4
11d	CF_3	H	**11.5** ± 0.6	**15.3** ± 0.5	45.1 ± 0.1	22.4 ± 0.3
11e	Cl	CH_3	**4.7** ± 0.8	**16.0** ± 0.6	34.8 ± 0.4	23.2 ± 0.5
11f	H	OCH_3	**9.9** ± 0.7	**14.6** ± 0.5	>100	16.9 ± 0.5
11g	H	CH_3	**2.1** ± 0.8	52.0 ± 0.4	17.8 ± 0.6	19.3 ± 0.5
11h	H	F	**0.97** ± 0.8	31.7 ± 0.2	18.9 ± 0.5	28.3 ± 0.4
11i	Cl	Cl	**3.6** ± 0.9	61.9 ± 0.4	14.6 ± 0.7	7.8 ± 0.8
11j	H	Cl	**7.7** ± 0.8	**28.9** ± 0.2	23.3 ± 0.4	11.6 ± 0.5
11k	CF_3	Cl	**12.1** ± 0.6	45.3 ± 0.2	28.0 ± 0.2	18.4 ± 0.5
11l	OCH_3	H	**6.8** ± 0.6	**28.4** ± 0.4	56.9 ± 0.3	67.7 ± 0.2

11m	F	H	**6.6** ± 0.9	64.1 ± 0.1	16.7 ± 0.6	13.7 ± 0.5
Sorafenib	-	-	15.5 ± 0.4	29.6 ± 0.3	6.4 ± 0.6	2.8 ± 0.8

[a] Values were the means of three replicates ± standard deviation (SD).

Table 2. In vitro cytotoxic effects (IC_{50}, μM) of compound **11i** against Hu02 cell line[a]

Compound	Hu02
11i	34.3 ± 0.3
Sorafenib	40.0 ± 0.5

[a] Values were the means of three replicates ± standard deviation (SD).

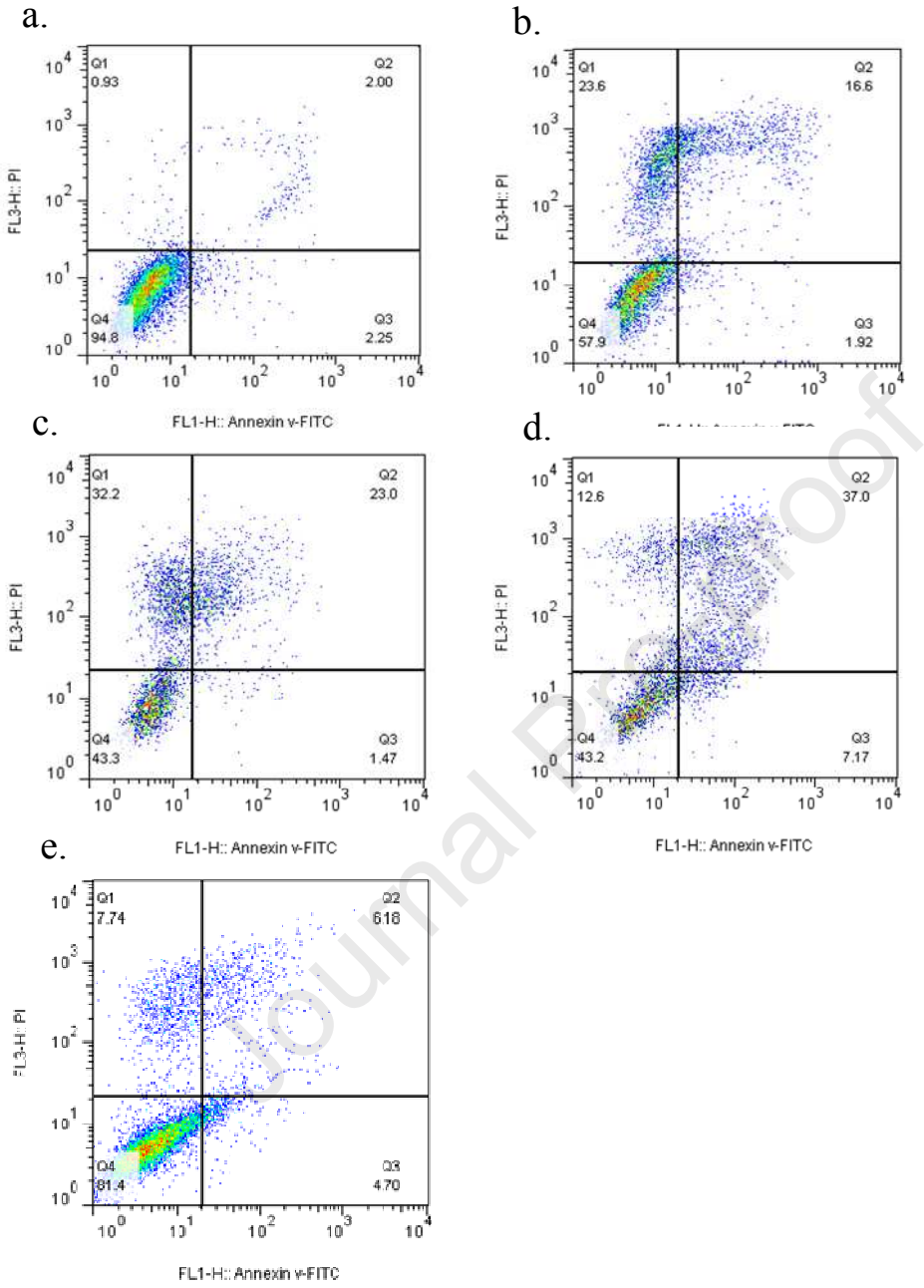

Fig. 3. Flow cytometry analysis of PC3 cells treated with compounds **11h** and **11i**. (a) Nontreated cells as negative control group; (b) treated with sorafenib as positive control at its IC_{50}; (c) treated with **11h** at its IC_{50}; (d) treated with **11i** at its IC_{50}; (e) treated with dimethyl sulfoxide as solvent. Early apoptotic cells (Annexin V-positive, propidium iodide-negative) appear in the lower right quadrant and late apoptotic cells (positive for both markers) in the upper right quadrant.

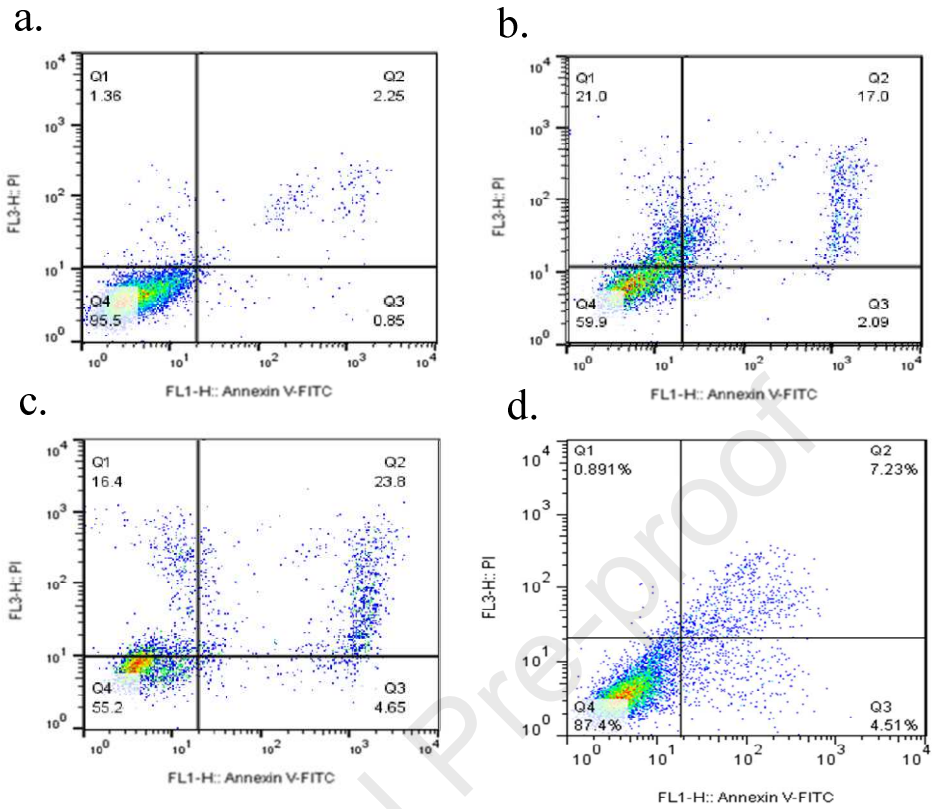

Fig. 4. Flow cytometry analysis of HUVEC cells treated with compound **11i**. (a) Nontreated cells as negative control group; (b) treated with sorafenib as positive control at its IC50; (c) treated with **11i** at its IC50; (d) treated with dimethyl sulfoxide as solvent. Early apoptotic cells (Annexin V-positive, propidium iodide-negative) appear in the lower right quadrant and late apoptotic cells (positive for both markers) in the upper right quadrant.

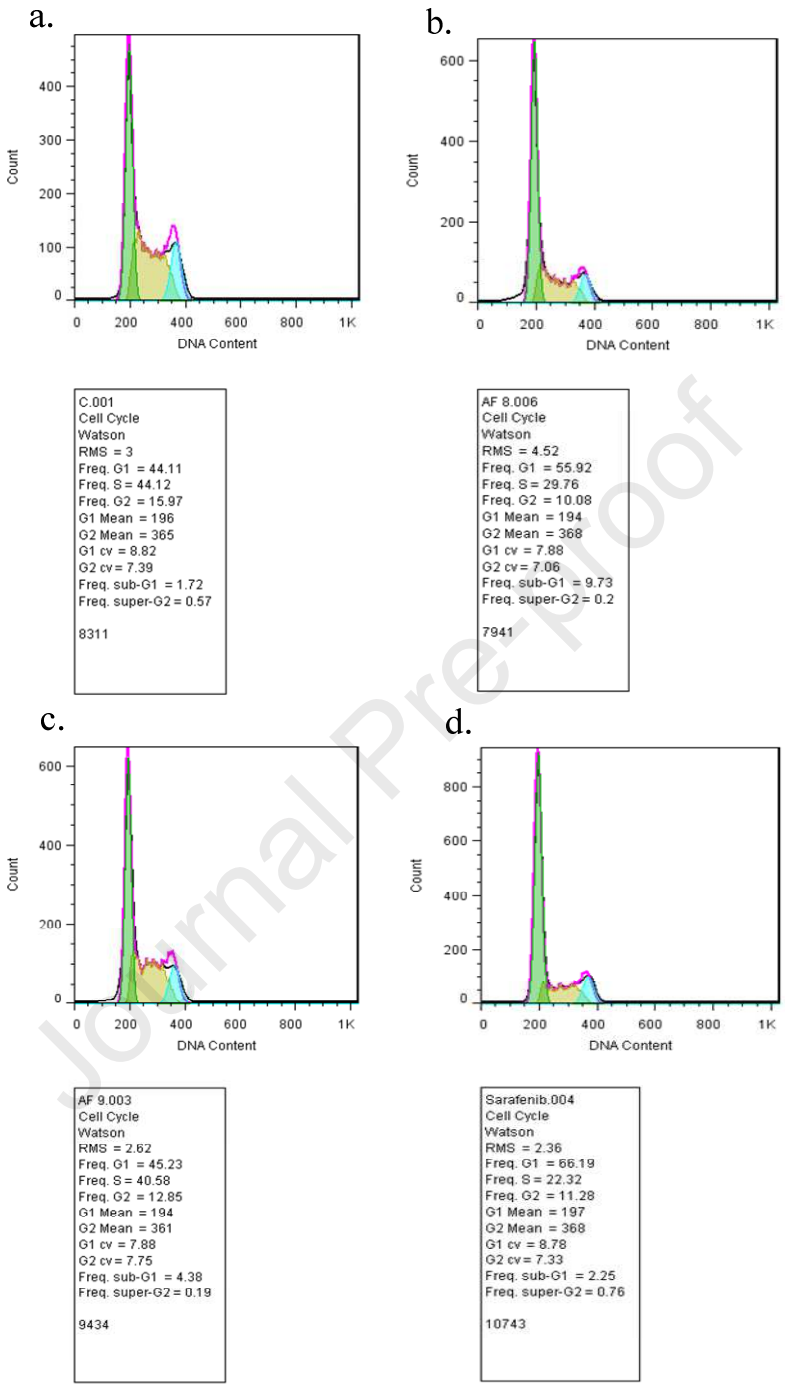

Fig. 5. Effect of compounds **11h** and **11i** on the cell cycle distribution of PC3 cells by flow cytometry analysis. (a) Non-treated cells as the control group; (b) treated with **11h** at its IC_{50}; (c) treated with **11i** at its IC_{50}; (d) treated with sorafenib at its IC_{50}.

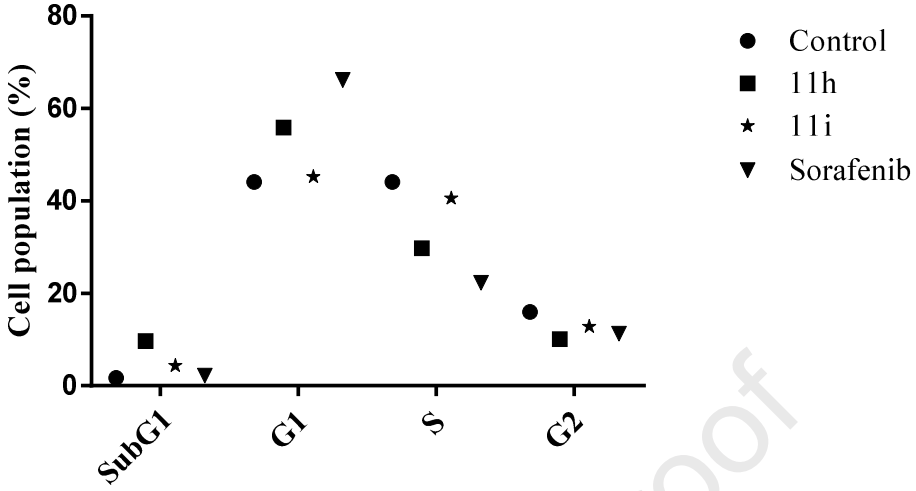

Fig. 6. Quantitative measurement of the cell cycle analysis.

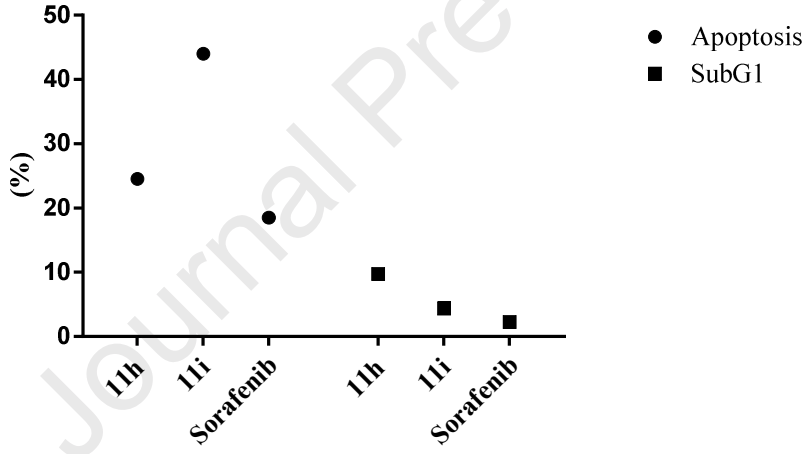

Fig. 7. The amount of apoptosis mediated by **11h**, **11i**, and sorafenib versus the cell population arrested in the subG1-phase. The graph was presented by separated symbols, trying to make a logical connection between the dependent variables.

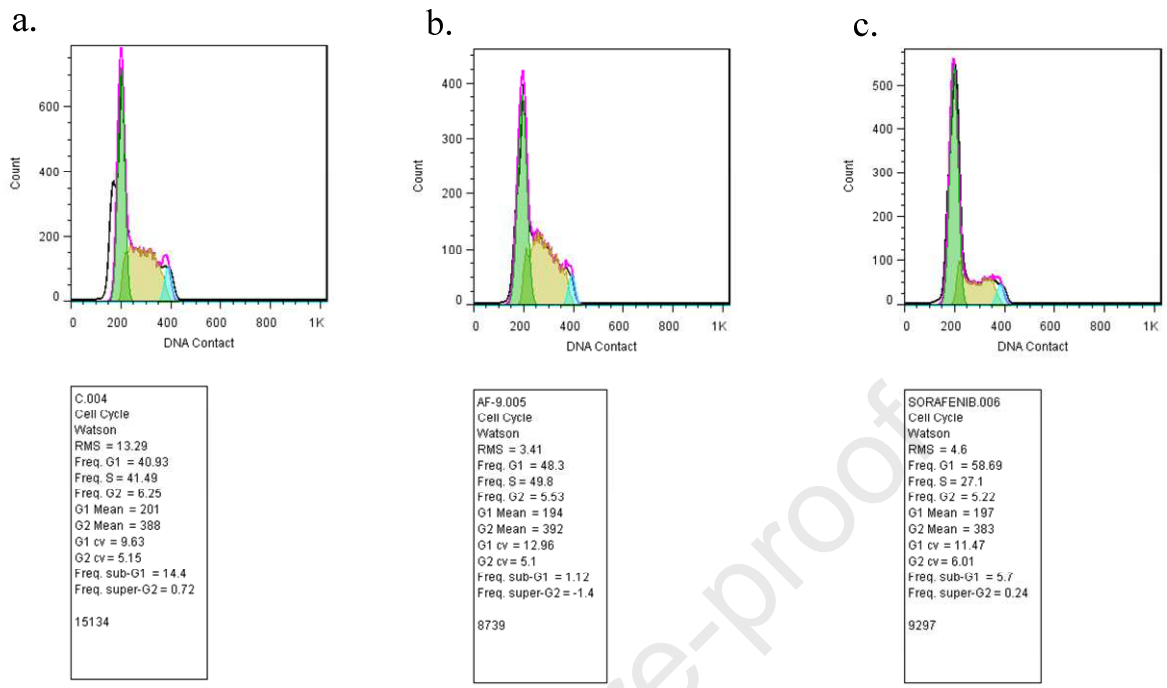

Fig. 8. Effect of compound **11i** on the cell cycle distribution of HUVEC cells by flow cytometry analysis. (a) Non-treated cells as the control group; (b) treated with **11i** at its IC_{50}; (c) treated with sorafenib at its IC_{50}.

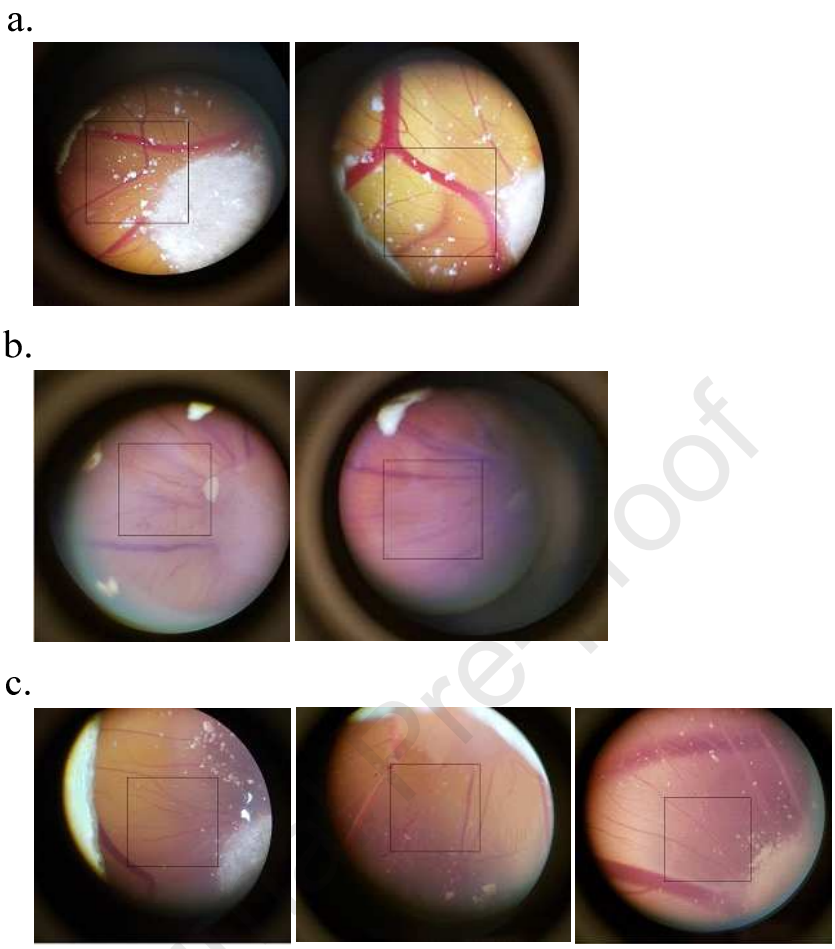

Fig. 9. Screening compounds by the chick chorioallantoic membrane (CAM) assay. (a) Negative control; (b) sorafenib; (c) **11i**.

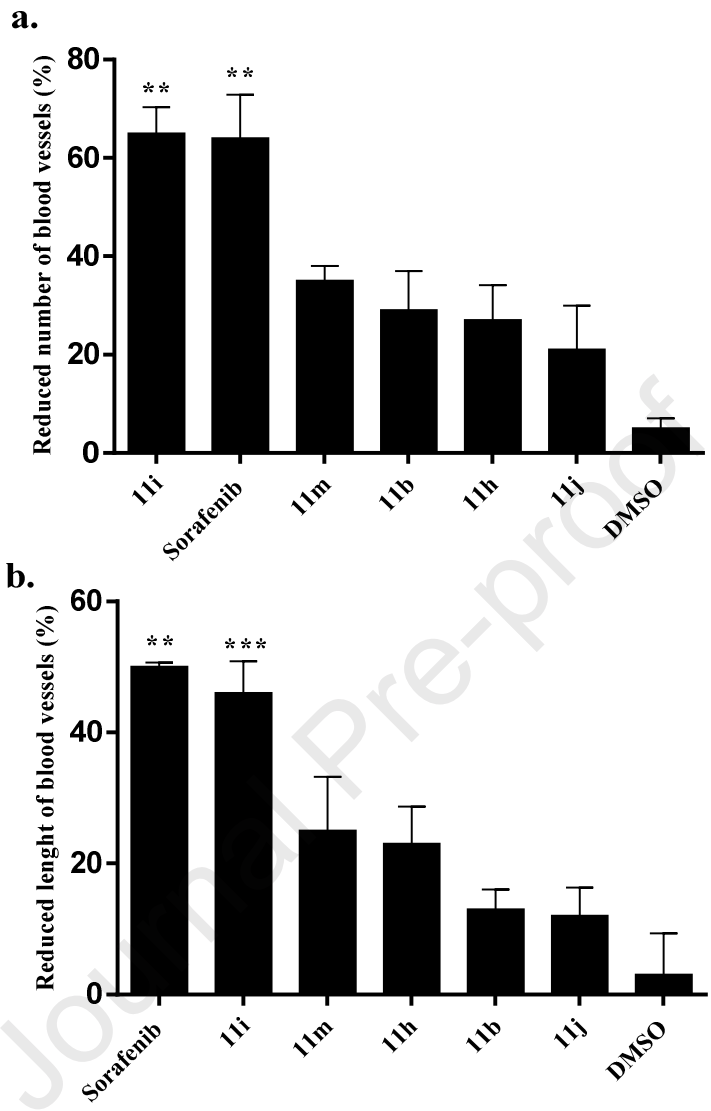

Fig. 10. a) Quantification of the effects of **11b**, **11h**, **11i**, **11j**, and **11m** on the number of CAM blood vessels. The bars show the mean ± SD (n=5). Statistical significance: **P < 0.01. b) Quantification of the effects of **11b**, **11h**, **11i**, **11j**, and **11m** on the length of CAM blood vessels. The bars show the mean ± SD (n=5). Statistical significance: **P < 0.01, ***P <0.001. **11i** concentration: 3.6 μM; sorafenib concentration: 15.5 μM.

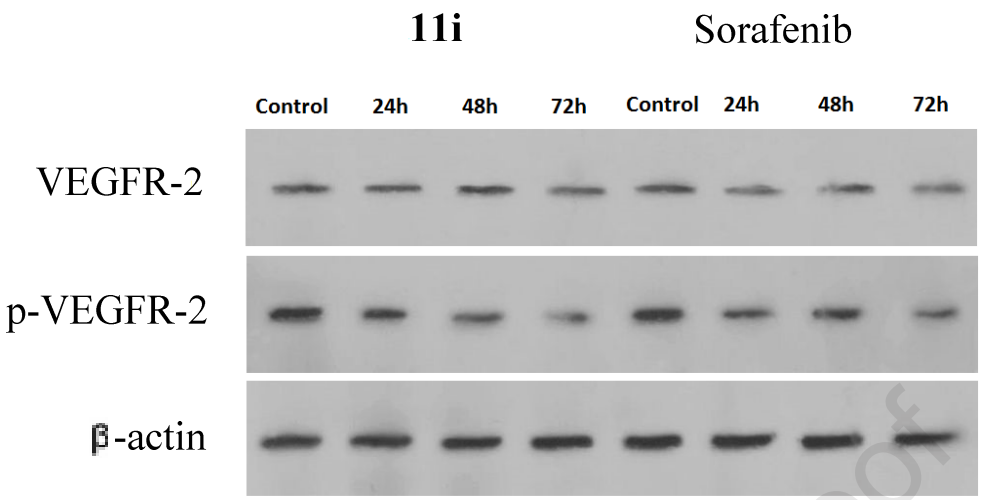

Fig. 11. Western blot analysis of **11i** and sorafenib on the VEGFR-2 phosphorylation in the PC3 cell line after 24, 48, and 72 h.

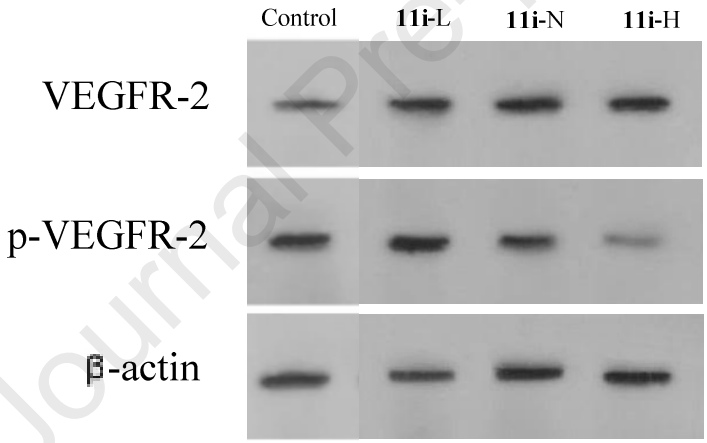

Fig. 12. Expression of VEGFR-2 and p-VEGFR-2 in PC3 cells treated with different concentrations of **11i** for 48 h. Control: treated with no drug; **11i**-L: treated with 2.4 μM **11i**; **11i**-N: treated with 3.6 μM **11i**; **11i**-H: treated with 5.4 μM **11i**.

a.

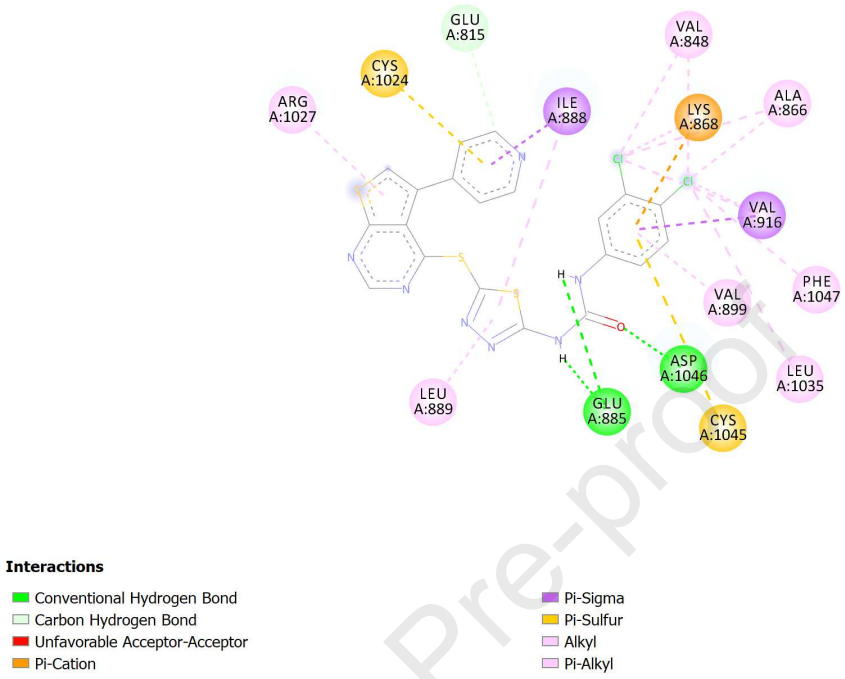

b.

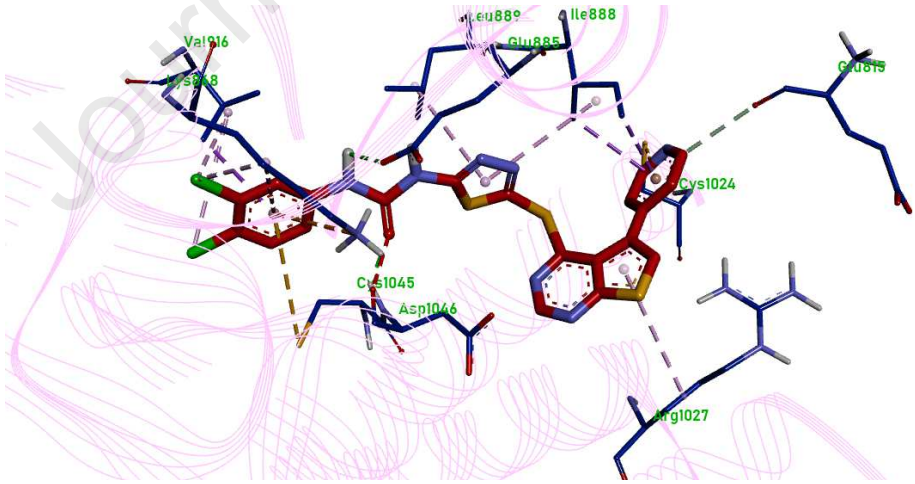

Fig. 13. a) 2D illustration of compound **11i** and the corresponding interactions with residues in the active site of VEGFR-2; b) 3D illustration of compound **11i** and the corresponding interactions with residues in the active site of VEGFR-2.

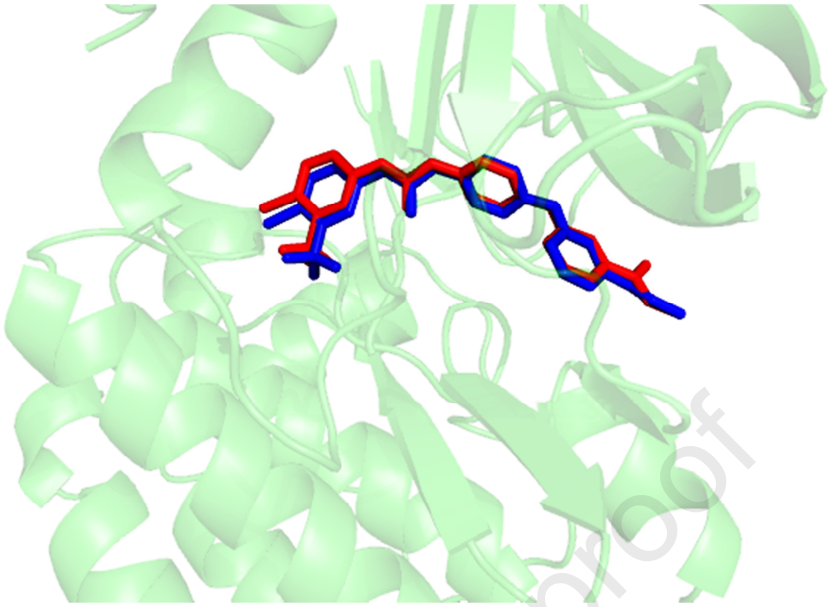

Fig. 14. Superimposed representation of redocking lowest energy poses into the co-crystalized ligand sorafenib over 3WZE.

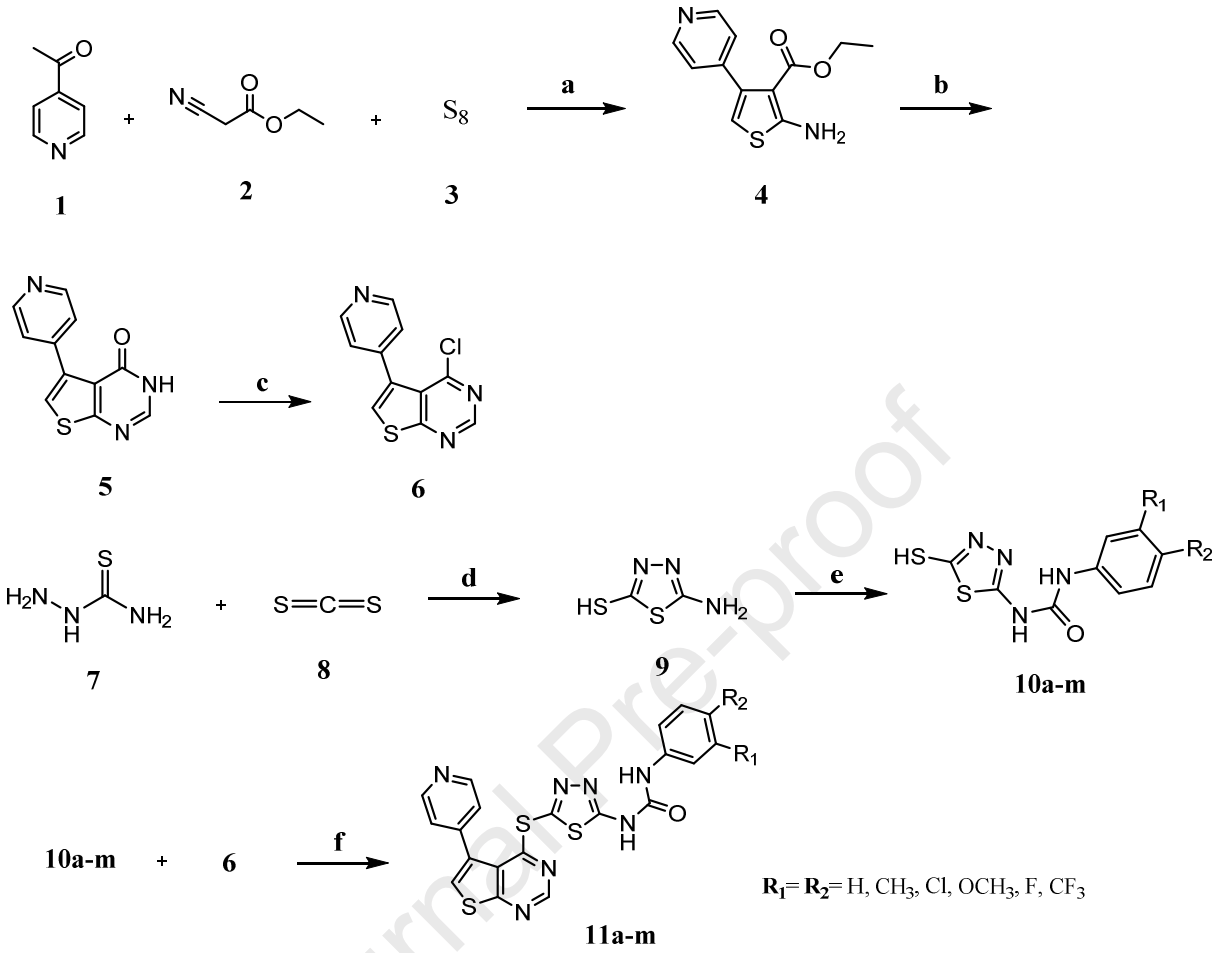

Scheme 1. Reagents and conditions: a) morpholine, reflux, 14 h, 70%; b) formamidine acetate, DMF, 100 ^{o}C, 16 h, 74%; c) $POCl_3$, DIPEA, 45 ^{o}C, 42%; d) sodium carbonate, dry EtOH, reflux, 8 h, 84%; e) various substituted phenyl isocyanate, dry DCM, rt, 24 h, 45-55%; f) KOH/EtOH, reflux, 6h, 60-68%.

- Thienopyrimidine-based compounds bearing the diaryl urea functionality were designed and synthesized.
- **11i** could inhibit the proliferation of PC3 cells by nearly 4-fold, respectively compared to sorafenib
- CAM assay revealed that the growth of blood vessels was inhibited by **11i** tremendously
- Western blot analysis of **11i** revealed the inhibition of VEGFR-2 phosphorylation

Declaration of interests

☒ The authors declare that they have no known competing financial interests or personal relationships that could have appeared to influence the work reported in this paper.

☐The authors declare the following financial interests/personal relationships which may be considered as potential competing interests: